

**U. S. Department of Commerce  
National Oceanic and Atmospheric Administration  
National Weather Service  
National Centers for Environmental Prediction**

**Office Note 446**

**NEAR-SURFACE DATA ASSIMILATION IN THE NCEP GRIDPOINT  
STATISTICAL-INTERPOLATION SYSTEM: USE OF LAND TEMPERATURE DATA  
AND A COMPREHENSIVE FORWARD MODEL**

Seung-Jae Lee<sup>1</sup>, David F. Parrish, and Wan-Shu Wu

NCEP/Environmental Modeling Center, Camp Springs, MD 20746

Oct 7, 2005

---

<sup>1</sup> Corresponding author address: Numerical Weather Prediction Division, Korea Meteorological Administration, 460-18 Shindaebang-Dong, Dongjak-Gu, Seoul, 156-720, Republic of KOREA  
E-mail: [sjlee@kma.go.kr](mailto:sjlee@kma.go.kr); Phone: 82-2-2181-0528; Fax: 82-2-836-5474

## Abstract

In this study, we use land surface temperature data in the NCEP regional Grid-point Statistical Interpolation (GSI) using the WRF-NMM model as a first guess. Single time analysis experiments are conducted to test the impact of land surface data on the analysis system and the results are compared with the control run without using land surface data. The effort is focused on understanding the characteristics of innovations (observed-guess) of the land surface data. Modifications to background errors and a simple test of nonlinear quality control will also be considered. The incorporation of a comprehensive near-surface observation operator into the NCEP regional GSI system is described. The comprehensive near-surface observation operator based on Monin-Obukhov similarity theory was tested for possible operational use. The results from this new forward operator are compared with those from the existing old forward operator.

According to the results, land surface mesonet temperature data were found to have a considerable amount of outliers compared with other land surface temperature data. The nighttime western and central domains indicated a model warm bias. Stations with large innovations are distributed uniformly in the nighttime western and central domains, while they are mainly located in the large cities in the daytime eastern domain. The statistical analysis of observation innovations showed that introduction of the new forward model can reduce bias and root-mean-square error in observation increment statistics. The results of short assimilation indicate that the new forward operator can be employed for near-surface data assimilation in the NCEP.

## 1. Introduction

The NCEP analysis system has gone through many changes since optimum interpolation (OI) became its main component in 1978 (Bergman 1979; Dey and Morone 1985; DiMego 1988; Kanamitsu 1989; Derber et al. 1991; Parrish and Derber 1992). Recently, the 3DVAR-Gridpoint Statistical-Interpolation (GSI) System was developed as the next generation global analysis system which uses recursive filters in grid point space to model the action of the background error covariance matrix upon the spatial distribution of observation increments (Wu et al. 2002, Purser et al. 2003). Furthermore, the current unified global/regional analysis system was developed after realizing that it was fairly straightforward to modify the GSI for both global and regional applications.

The NCEP GSI analysis system can assimilate diverse kinds of observation data such as synoptic, satellite, and radar data. Especially, as the importance of and demand for real-time mesoscale analysis (RTMA) grows in the world of weather forecasting, near-surface data assimilation becomes one of the challenges to conquer. Efforts for analyses of the atmosphere at high spatial and temporal resolution with particular attention placed on weather and climate conditions near the surface are on-going in the Analysis of Record project (DiMego et al. 2005). This mesoscale surface analysis is expected to greatly contribute to improvements in short-range model forecasts and forecasters' analysis of mesoscale weather. The United States has high-resolution observation networks over land, and surface observation data are abundant. For example, the U. S. meso-network systems measure and provide useful information on the environment at the size and duration of mesoscale weather events.

In spite of abundant near-surface observations, however, it is not easy to assimilate them into numerical weather analysis and prediction system practically. It is because of following reasons (COMET program 2005): Other data are needed to get vertical structure. There is no good way to infer the 3-D structure associated with, for instance, a lower than predicted surface pressure. As a result, the data influence fades away during the forecast; Near-surface observations may harm the boundary-layer structure in the model if not introduced with care; Surface stations may be at different heights than the model topography, causing problems for all observed variables but

especially surface temperature; An inhomogeneous distribution of observations complicates objective analyses of near-surface variables; There is an uncertainty in observation error and correlation between the background errors for any pair of grid points is independent of location; Observation operators are not accurate. There have been diverse studies (e.g., Doswell and Lasher-Trapp 1997; Guo et al. 2002, Myrick et al. 2005) to solve or relieve these kinds of problems. Wade (1987) verified the quality of surface mesonet data collected during the Cooperative Convective Precipitation Experiment (CCOPE). His results showed observed temperature and wind speed differences between the two mesonet systems used in the CCOPE.

In the GSI system, the observation operator, called the forward model, converts the analysis variables to the observation type and location. These forward operations from the background to the observation may include variable transformations in case of, for example, radar or satellite data assimilations. The quality of the simulated observation, the model state converted to "observation units", depends significantly on the accuracy of the forward operator. Concerning observation operators, Urban (1996) derived observation operators for land surface data assimilation. Ruggiero et al. (1996) and Ruggiero et al. (2000) used their forward operator for intermittent assimilation of hourly near-surface observations. Guo et al. (2002) developed a new observational operator and its corresponding adjoint to assimilate automatic weather station (AWS) observations, which is high-resolution (about 15 km) near-surface data of the Korea Meteorological Administration (KMA). They showed that 3DVAR assimilation of high-resolution KMA AWS data could improve the model skill in short-range prediction of a heavy precipitation case over the Korean Peninsula. For near-surface observations, Benjamin (2004) used a surface-layer similarity model to match 2-m temperature and moisture observations and 10-m winds to the Rapid Updated Cycle background whose lowest level is at 5 m above the surface. However, there is no near-surface model in the NCEP GSI system. Currently, the forward model in the NCEP GSI system just involves simple interpolation of the background value to the location of the observation. The assumption in this case is that the model has sufficient resolution to define an atmospheric boundary layer which can be interpolated directly to the observation. If this is a bad assumption and boundary layer parameterization is required, simple interpolation will generate inaccurate

pseudo-observations, increasing the error in observation increments and degrading the analysis.

In this study, we carry out assimilation experiments of land surface temperature data in the NCEP regional GSI system. The effort is focused on understanding the characteristics of innovations (observed–guess) of the surface mesonet data. Single time analyses are conducted and modifications to background errors are considered. A simple test of nonlinear quality control (QC) will be presented. Also, in order to improve surface data assimilation for mesoscale analysis, a new forward operator was introduced into the NCEP GSI system. Some preliminary results of testing the comprehensive near-surface observation operator based on surface-layer similarity theory are presented for possible operational implementation.

In section 2, the near-surface data used and experimental design are described with results and discussion for use of land surface temperature data. In section 3, we present a detailed description of the comprehensive forward operator and results for application of it. Finally, summary and present plans for future work will be provided in section 4.

## **2. Use of land surface temperature data**

### *a. Data and experimental design*

#### 1) NEAR-SURFACE DATA AND QUALITY MARKERS

In the current operational regional analysis and forecast system, all mesonet data are not assimilated and the observation error for all mass (temperature, surface pressure, moisture) and wind observations is unknown. The mass data for a mesonet report is stored under PREPBUFR report type 188 and the wind data is stored under PREPBUFR report type 288. Because the observation error is missing, an extra "layer" of QC is added in the PREPBUFR processing. This QC sets the quality marker to "9" for surface pressure, temperature, specific humidity and wind. Previously the quality markers for these data were either "1" (for good), "2" (for neutral or not checked) or "3" (for suspect). A higher quality marker indicates a lower observation quality. All quality markers of 4

and higher (4-15) are considered "bad" (for various reasons) and the observation will not be assimilated.

We at NCEP currently do not perform any automated platform-specific QC on mesonet or any other surface data. There are good, neutral, suspect or bad quality markers on the data as it comes in based on the FSL-MADIS QC. In addition, NCEP could (but currently doesn't) place manual quality markers on the mesonet data (either "0" for keep or "14" for purge). This would be done by either putting reports on a reject list that might be updated monthly or on a report-by-report basis by the NCEP Senior Duty Meteorologist (SDM) who works in NCEP Central Operations. Also, we perform some gross checks and flag data that are outside reasonable limits, data with missing latitude or longitude, etc. Since the observation error is missing in operations, all mesonet data get a quality marker of "9" and the analysis then skips over them even though they are in the operational PREPBUFR files.

In this study, we modify the observation error file to assign the mesonet observations in PREPBUFR report types 188 and 288 the same observation error as for METAR mass and wind observations in report types 187 and 287, respectively. Clearly, this procedure is somewhat arbitrary, but it is adopted due to the lack of information regarding the observation error for mesonet data. NOAA FSL, for example, assigns to mesonet data the error values used for other surface data but inflates it by a factor of 1.5. In our special runs, we are making PREPBUFR files identical to the operational ones, except the observation errors for the mesonet data are now not missing. In this case, the extra layer of QC does not occur. The original quality markers are retained for the mesonet data, so the analysis will assimilate all mesonet observations that do not have a bad quality marker due to the original MADIS QC. The time window over which data collection is performed is +/- 70 minutes at 00 and 12 UTC, and +/- 50 minutes at 06 and 18 UTC. The 3DVAR analysis is valid at center of time window.

## 2) MODIFICATION TO BACKGROUND ERROR STATISTICS

Up to now, in the NCEP GSI, the background error for regional assimilation has been a downscaled version from the background error derived from the global model. The downscaling is just an interpolation but we have tuning coefficients for amplitude,

horizontal and vertical scales. Recently, Wu (2005) has estimated the background error statistics for NCEP's regional forecast model WRF-NMM. The NMC method is used to estimate the background error from forecasts of an 8 km WRF-NMM over the "central" US domain. According to the results, the horizontal scales of the structure function derived from the horizontal gradients of the forecast differences were very unstable and change sharply from layer to layer. She suggested that the problem of the statistics might be related with the high resolution and non-hydrostatic model. She also found that auto-correlation is the most stable and robust in estimating the horizontal structures among the new methods tested. Applying auto-correlation to the entire horizontal domain, however, means that the scale statistics are now only height dependent. Figure 1 shows the vertical cross sections of the temperature and corresponding east-west wind analysis increments resulting from a single temperature observation with 1 °C observational residual for downscaled global and regional background errors. Note that we don't expect geostrophy near the surface because of the forcing is not limited to pressure and Coriolis force (earth rotation). The response near the surface is just the result of the statistic character of the fields that contain information of friction, terrain, diabatic heating etc.

### 3) NON-LINEAR QC PROCEDURE

The GSI contains an option to perform nonlinear QC (Andersson and Järvinen, 1999). This is currently used in the operational North American Data Assimilation System (NDAS). The version in the parallel WRF-GSI NDAS has not been activated yet. In these experiments, some preliminary results are presented using nonlinear QC. The idea behind nonlinear QC is to modify the assumption of Gaussian error statistics for observation error, which is currently made in most operational variational data assimilation systems. The simplest modification, which is used operationally and in GSI, is to add a constant to the Gaussian distribution of error, which implies that the probability of the value of an observation being incorrect is equally distributed over the range of observed – analysis values bounded by the assumed gross error limit. So there are three parameters used in GSI to characterize the error distribution, which are defined for each observation type—1) the gross error limit, 2) the observation error standard deviation, and 3) the probability that an observation is a gross error. The names of the

parameters are “gross”, “var\_b”, and “var\_pg”, respectively, in the GSI. The “gross” is the gross error checking parameter, where an observation is rejected if  $|\text{innovation}| > \text{gross} \times (\text{observation error})$ . The “var\_b” is the expected range of observation innovation, which, if the observations have been checked for gross error, means that  $\text{var\_b} = \text{gross}$ . The var\_pg is the probability of an observation being a gross error. All observations are screened against the background and eliminated if the difference exceeds the gross error limit. Then, during the minimization to obtain the analysis, the effective weight given to an observation depends on the difference between the evolving analysis and observed values. For this to work properly, a good estimate of the analysis must be obtained prior to turning on the nonlinear QC, using observations screened against the background with the gross error check. For the experiments reported here, using nonlinear QC, 50 iterations are performed without nonlinear qc to get a first estimate of the analysis, and then 50 more are carried out with nonlinear qc, in which observations that are inconsistent with nearby observations are rejected.

In this study, therefore, the effect of the new regional background error was examined as well as sensitivity of regional GSI system to land surface temperature data. A preliminary test using the nonlinear QC algorithm will also be shown. Table 1 shows the experimental design based on what has been described above. The NCEP WRF-NMM 8 km forecasts are used as background fields. There are three domains available for the WRF-NMM 8 km model: 3 hour-forecast first-guess fields for the western, central, and eastern domains are at 06, 12 and 18 UTC respectively. Experiments are carried out for each model domain (Fig. 2). The background error estimated from the central domain is used in all three domains. The background error covariance is assumed to be as about the same among them because the three domains cover about the same latitudes and the error covariance is mainly function of latitude.

## *b. Results and discussion*

### 1) ANALYSIS COMPARISONS

In Fig. 3, we show satellite and radar images (overlapped with the surface analyses) at 0600 UTC 14 Feb, 1200 UTC 10 Mar, and 1800 UTC 23 Mar 2005. They are

all produced and issued regularly by the National Oceanic and Atmospheric Administration.

At 0600 UTC 14 Feb 2005, the weather was very clear over most of the western USA domain and did not show any precipitation at this nighttime (Fig. 3a). Figure 4 shows the result for a single analysis on the western domain, valid 0600 UTC 14 Feb 2005. The control run (CNTL) showed negative analysis increments (AN1-GES) below magnitude of about 2°C and comparatively large analysis increments along the western coast. Addition of synoptic land data (SYNP) has small impact mainly in land and the overall pattern is similar to CNTL. Addition of METAR or mesonet temperature data generates much different pattern of analysis increments from CNTL. With use of METAR data, the big negative analysis increments are located not in coastal area but in land, especially, the Rocky mountain area in Wyoming, Colorado and New Mexico. The result for use of mesonet temperature data has similar structure with that for use of METAR data, but more intensified and organized. The excessive amplification is related with the number and spatial density of each type's data: Approximately, the number density has a ratio of 1 : 2 : 14 : 173 which corresponds to synoptic sea, synoptic land, METAR, and mesonet data, respectively. The difference between experiment MESO and ALLD is comparatively negligible. In this case, moreover, the model first-guess performance was bad and worsened the analysis results leading to abnormally large analysis increments. The large differences between the analysis and guess fields are very much what one would expect, and stress the problems we currently have with attempting to use surface temperature data. For this case, because of the clear nighttime inversion over much of the domain, the observations are consistently colder than the model, leading to the large negative analysis – guess at the surface.

Figure 5 shows the result for a single analysis on the central domain, valid 1200 UTC 10 Mar 2005. The weather was clear sky conditions with strong surface temperature inversion in the early morning (0700 LST, Fig. 2b). Use of synoptic land data does not produce difference from CNTL except for a little impact in Indiana and the boundary between Texas and Louisiana. It can be seen that the analysis field has smaller and detailed structures as METAR or mesonet data are added: Noticeably, positive analysis increments are created by the inclusion of METAR or mesonet data in the northern-

central region where the low pressure system is located in Fig. 3b. This implies a regional warming effect by precipitation (rain) over the comparatively cold land surface can be accounted for with the METAR or mesonet data included. There is a shift of negative analysis increment axis over the Rocky mountain areas between experiments META and MESO.

Figure 6 shows comparisons of analysis field against radiosonde soundings in the central US domain at 12 UTC. For the comparison, analysis fields are interpolated to the radiosonde points. Note that there can be some differences between background and radiosonde profiles since only near-surface temperature data are used in this study. On the whole, the figure demonstrates that use of land surface temperature data has positive effects on the vertical profile of analysis field. In case of MIa, use of METAR or mesonet data moves the background toward the observed radiosonde profile resulting in a good agreement below 930 hPa. The MI d shows background profile is gradually changed toward radiosonde sounding as much land temperature data are used as possible (Radiosonde data at the surface were missing in this case). The MN radiosonde site, which is located in the low pressure system area with precipitation, shows background boundary layer is corrected toward warmer boundary layer. In case of AZ, surface pressure is comparatively low since it is located in Rocky mountain area. The first-guess field does not have any information about the occurrence of low level nighttime inversion and has a discrepancy from radiosonde sounding above 900 hPa. With the addition of METAR data, the background becomes close to radiosonde data at the surface. TX also shows use of mesonet data helps analysis profile to be matched with radiosonde at the surface. In case of IL and LA, the pattern of analysis profile is opposite with radiosonde in the lower atmosphere, still use of METAR or mesonet data tends to reduce the difference at the surface.

When the entire vertical profile of the background field is far from the radiosonde observation, assimilation of land surface temperature data has an obvious effect at the surface. But use of only land surface data can not correct the boundary layer profile realistically. It can be attributed to not only not assimilating radiosonde observation, but also not considering of anisotropic and localized background error statistics, such as stability- and topography-dependent background error. Wu (2005) showed that the

variances and the structure functions from a different forecast system can be tuned to produce comparable analysis results except where the vertical grid resolutions are very different. If we consider the anisotropic and inhomogeneous background error, along with tuning of horizontal and vertical correlation lengths, more vertically consistent (or vertically connected) profiles would be obtained.

Figure 3c shows the daytime (1400 LST) eastern case where a low-pressure system is located over the eastern coast. Although we cannot know much about the background until we do some assimilation experiments, even in the east coast case, the analysis - background is large (Fig. 7). It just has smaller scales, reflecting the fact that there is a low with a large amount of local variation, whereas the west situation was characterized by a clear nighttime stable surface layer, which at least in this case was very large in scale.

Left-column panels in Fig. 8 show analysis differences between AN4 using global and regional background error statistics. When the regional background error statistics are used, the overall analysis increment becomes more intensified in all the domains. It is believed to be the results of smaller vertical structures in the regional background error covariances (Fig. 1).

Right column panels in Fig. 8 show results for use of nonlinear QC procedure that is available in the NCEP GSI system. The nonlinear QC was turned on during the entire second outer loop. The three parameters “gross”, “var\_b”, and “var\_qc” are given by 10, 10, and 0.08, respectively. It can be seen that nonlinear QC contributes a little bit to reduction of excessive analysis increment in the figure. However, because of the coherent large scale bias in observed – background, the observations tend to agree with each other. The nonlinear QC procedure primarily removes observations that don’t agree with nearby observations.

## 2) OBSERVATION INNOVATIONS: ACCUMULATED STATISTICS

Observation increments are the differences between observed data and background data after the background data have been converted to simulated observations by space and time interpolation and variable conversion. In order to identify the source of the large analysis increments, an attempt was made to look at the

temperature increments (observed - guess) for the mesonet data. In the GSI, if the pressure of the observed surface temperature is less than the guess pressure at sigma level 1, then the guess temperature is interpolated in the vertical to the observed pressure. If the pressure of the observed surface temperature is greater than the guess pressure at sigma level 1, then the guess temperature is the value at sigma level 1. If an observation is outside the range of model sigma levels, the interpolated value is replaced by the value of the sigma level closest to the observation. To see if the large apparent difference bias between observed and guess results from extrapolation outside the model domain, the observations are divided into those where (1) the observed pressure is less than the sigma 1 guess pressure, in which case the guess temperature is interpolated to the observed pressure; and (2) all remaining observations where observed pressure is larger than the sigma 1 guess pressure. We looked at the average of (observed - guess) for both cases.

Figure 9 displays the scatter diagram of observed versus first-guess surface temperature ( $^{\circ}\text{C}$ ) during May 2005 for the night-time (0600 UTC) western, dawn-time (1200 UTC) central, and day-time (1800 UTC) eastern domains. It is found that surface mesonet temperature data have a considerable amount of outliers compared with other type of land surface temperature data, i.e., METAR and synoptic data. Such outliers imply not only bad observations but also local effects. In case of mesonet temperature data, some stations can be seen to produce the same values regardless of model forecasts. Generally, mesonet “wind” data have not been used in the data assimilation system based on the clear evidence for widespread siting problems (Benjamin 2005, personal communication). 5/6 of all mesonet data are from AWS (Automated Weather Source), which includes most school sites, and APRSWXNE (citizen’s network). It is confirmed that the siting for these networks are poor, so that knocks out most of the mesonet data right there (Horel 2005, personal communication). Also it is known that in site of buddy check on differences from background values, if there are systematic errors within a network, mesonet winds often (not always, probably depends on subprovider) drastically underestimate wind speed (Manikin 2005, personal communication). In this study, it is confirmed that quality markers placed on the mesonet data by the FSL-MADIS QC can be of little value not only for wind but also temperature data. A short-term approach to fix this problem is to set up the mesonet uselist (or reject list) using mesonet provider or

subprovider lists and this is on-going with monitoring with observed-background data on a station-by-station and variable-by-variable basis (Benjamin 2005, personal communication).

Figure 10 shows comparison of observation increment statistics among the domains for surface temperature data during May 2005. The slope and correlation coefficients ( $r^2$ ) of land surface temperature data are good and similar in all three domains. However, in the case of synoptic sea surface data, they show a peculiar pattern in the western domain (see Fig. 9d): a steep slope and very low correlation coefficients below 0.5. This seems to be caused by the fact that buoy observations are easily affected by sea surface conditions and ocean waves. As for the land surface temperature data, the nighttime western domain shows the worst RMSE among the three domains. In the case of synoptic sea surface data, the eastern domain shows the worst RMSE and the western domain the lowest correlation coefficient.

Figure 11 shows the mean innovations for the surface temperature data as a function of surface pressure difference between model and observation for the month of May 2005. The nighttime western and central domains indicate a model warm bias. The western domain, in particular, shows a model warm bias of about +2.2 °C at nighttime when compared with the eastern domain which did not show any obvious bias. The o-g statistics as a function of surface pressure difference in the eastern domain seems to indicate that the mesonet observations have small temperature bias (about +0.5 °C).

The number of stations as a function of surface pressure difference in the western domain revealed an asymmetric distribution implying there are many stations where the model surface is higher than the observation surface (Fig. 12). This could partly account for the model warm bias in the western domain at nighttime. In the other two domains, the distributions are comparatively axisymmetric (Lee et al. 2005).

In the GSI, if the observation surface elevation is too far from the model elevation, the observation error is smoothly increased. From Figs. 9-12, we can think about expected range of (observed – guess) and surface pressure difference for near-surface temperature data: Valid values are about 7 °C for gross error checking parameter, which is currently set to 10 °C, and 5 hPa for surface pressure difference. These proposed limits could be used in order to effectively reject data.

Figure 13 shows large innovation sites in each domain during May 2005. Unlike the other two types of surface stations, surface mesonet stations are very dense, particularly around large cities (Figs. 13a, c, and e). Stations with large innovations are distributed uniformly in the nighttime western and central domains, while are mainly located in the large cities in the daytime eastern domain (Figs. 13b, d, and f). In the case of the eastern domain, it is 14 LST and the synoptic situation is characterized by many local and unstable situations with small-scale variation in daytime. In the case of the western (central) domain, it is midnight (dawn) and frequent large-scale inversion situation prevail. Therefore, it seems that the observations are not bad in western and central domains, but the model was perhaps in error in all domains as deduced from the homogeneous distributions of large (o-g) stations. These differences could also be the result of urban heat island effects (not contemplated in the model) or erroneous station groups.

### 3. Introduction of a new near-surface forward operator

The National Centers for Environmental Prediction (NCEP) GSI analysis system minimize an objective function (Kimeldorf and Wahba 1970, Lorenc 1986) given by

$$J = \frac{1}{2} [x^T B^{-1} x + (Hx - y)^T (O + F)^{-1} (Hx - y)], \quad (1)$$

where  $x$  is an  $N$ -component vector of analysis increment;  $B$  is the  $N$  by  $N$  previous forecast-error covariance matrix;  $O$  is the  $M$  by  $M$  observational (instrumental)-error covariance matrix;  $F$  is the  $M$  by  $M$  representativeness (forward operator)-error covariance matrix;  $H$  is a linear or nonlinear transformation operator;  $y$  is an  $M$ -component vector of observational residuals; that is,  $y = y_{obs} - Hx_{guess}$ ;  $N$  is the number of degrees of freedom in the analysis; and  $M$  is the number of observations.

The accuracy of an analysis is dependent on the effectiveness of the algorithm used to match observations with the background values for calculation of observation-minus-background innovations (Benjamin et al. 2004). The current near-surface

observation operator in the NCEP GSI system was improved from a simplified linear interpolation in space to a more comprehensive similarity model. The new forward model based on Monin-Obukhov similarity theory has been tested and compared with the results from the existing simple forward model. Particular attention has been given to the difference between “simulated observations” and the actual observations.

There does not exist forward, tangent-linear and adjoint models corresponding to all available boundary and/or surface layer physics we can choose as an option in a NWP model. In this study, as a first step, we introduce a new comprehensive forward operator for near-surface meteorological variables into the NCEP regional GSI system and evaluate its performance and usefulness especially with the hope that this could be a way to fix the systematic errors the existing system has in observation innovation statistics.

The new observation operator was originally developed for the MM5 3DVAR system (Barker et al. 2004). It uses a similarity theory based on Dyer and Hicks (1970) formula which has been adopted in the model PBL parameterization such as surface layer process in MRF PBL scheme (Hong and Pan 1996). It has also been used for surface data assimilation in operational analysis systems and has proven to be encouraging in many contexts like forecasts of heavy rainfall and typhoon track. (e.g., Guo et al. 2002; Shin 2004, personal communication; Hwang 2005, personal communication). Unlike the existing forward operator, this new forward operator assumes all the surface observation sites are located at the model surface, regardless of the actual difference in elevation between the surface measurement and the model surface. The different types of surface observations are directly assimilated without any modification. The observed surface pressure is still reduced to the model’s lowest level. With this new forward model, near-surface wind and mass variables are obtained at different heights using the surface layer similarity theory: Near-surface wind is obtained at 10 m, while temperature and specific humidity are obtained at 2 m. The following is a detailed description of the forward model.

#### *a. Forward model description*

10-m wind ( $U_z$ ,  $V_z$ ) is calculated from the lowest model levels using similarity

theory of the surface layer:

$$U_z = U_s \times \frac{\psi_{Wz}}{\psi_W} \quad \text{and} \quad V_z = V_s \times \frac{\psi_{Wz}}{\psi_W}, \quad (2)$$

where  $U_s$  and  $V_s$  are wind components at the lowest sigma level of the model.  $\psi_W$  and  $\psi_{Wz}$  are profile functions at the lowest sigma level and height  $z$ , respectively, and are given by

$$\psi_W = \log\left(\frac{h_s}{z_0}\right) - \psi_m \quad \text{and} \quad \psi_{Wz} = \log\left(\frac{z}{z_0}\right) - \psi_{mz}, \quad (3)$$

where  $h_s$  is the height of the lowest model level,  $z_0$  is the roughness length, and  $z=10$  m. On the other hand, mass variables ( $T_z$  and  $Q_z$ ) are obtained at 2 m height using the similarity theory as follows:

$$T_z = \left[ \theta_g + (\theta_s - \theta_g) \times \frac{\psi_{Tz}}{\psi_T} \right] \left( \frac{P_{sfc}}{1000} \right)^{R/Cp} \quad \text{and} \quad (4)$$

$$Q_z = \left[ Q_g + (Q_s - Q_g) \times \frac{\psi_{Tz}}{\psi_T} \right], \quad (5)$$

where  $\theta_s$  and  $Q_s$  are potential temperature and mixing ratio at the lowest sigma level, and  $\theta_g$  and  $Q_g$  are those at the ground.  $P_{sfc}$  is surface pressure and stability functions are given by

$$\psi_T = \log\left(\frac{h_s}{z_0}\right) - \psi_h, \quad \psi_{Tz} = \log\left(\frac{z}{z_0}\right) - \psi_{hz}, \quad (6)$$

$$\psi_Q = \log\left(\frac{ku_* h_s}{K_a} + \frac{h_s}{z_{q0}}\right) - \psi_h, \quad \text{and} \quad \psi_{Qz} = \log\left(\frac{ku_* z}{K_a} + \frac{z}{z_{q0}}\right) - \psi_{hz}, \quad (7)$$

where roughness length for water vapor ( $z_{q0}$ ) is prescribed as 0.01 m over land and  $z_{q0} = z_0$  over sea. Background molecular diffusivity ( $K_a$ ) is  $2.4 \times 10^{-5} \text{ m}^2\text{s}^{-1}$ , ideal gas constant ( $R$ ) is  $287.04 \text{ JK}^{-1}\text{kg}^{-1}$ , and specific heat at constant pressure ( $C_p$ ) is  $1004.0 \text{ JK}^{-1}\text{kg}^{-1}$ .

The quantities  $\psi_{m,mz}$  and  $\psi_{h,hz}$  are stability functions for momentum and heat, and are determined according to atmospheric stability which has the following four regimes based on Bulk Richardson number ( $Ri_b$ ).

1) STABLE ATMOSPHERE ( $Ri_b \geq 0.2$  )

$$\psi_m = -10 \times \log\left(\frac{h_s}{z_0}\right) \text{ and } \psi_{mz} = -10 \times \log\left(\frac{z}{z_0}\right). \quad (8)$$

2) DAMPED MECHANICAL TURBULENCE ( $0 < Ri_b < 0.2$  )

$$\psi_m = \frac{-5Ri_b}{1.1 - 5Ri_b} \times \log\left(\frac{h_s}{z_0}\right) \text{ and } \psi_{mz} = \frac{-5Ri_b}{1.1 - 5Ri_b} \times \log\left(\frac{z}{z_0}\right). \quad (9)$$

3) FORCED CONVECTION ( $Ri_b = 0$  or ( $Ri_b < 0$  and  $\theta_{v2} > \theta_{v1}$ ))

$$\psi_m = \psi_{mz} = 0. \quad (10)$$

Here, subscripts 1 and 2 mean the lowest and the second lowest sigma levels, respectively. For the above three regimes,  $\psi_m \geq -10$  ( $\psi_m = 0$  in case of free convection below),  $\psi_h = \psi_m$ , and  $\psi_{hz} = \psi_{mz}$ .

4) FREE CONVECTION ( $Ri_b < 0$  )

In case of free convection regime, stability functions have different formulas for momentum and heat. Stability functions are calculated using  $h/L$  which is a ratio of arbitrary height in surface layer to Monin-Obukhov length ( $L$ ):

$$\psi_m(x) = 2 \log\left(\frac{1+x}{2}\right) + y - 2 \tan^{-1}(x) + 2 \tan^{-1}(1.0), \quad (11)$$

$$\psi_h(x) = 2y, \quad (12)$$

where

$$x = \left(1 - 16 \frac{h_s}{L}\right)^{1/4} \quad \text{and} \quad y = \log\left(\frac{1+x^2}{2}\right); \quad (13)$$

$$\frac{h_s}{L} = \begin{cases} Ri_b \log\left(\frac{h_s}{z_0}\right), & \text{if } u_* < 1/100 \\ k \frac{gh_s}{\theta_s} u_*^{-2} \left(\frac{m}{L}\right), & \text{if } u_* \geq 1/100 \end{cases}, \quad (14)$$

where

$$Ri_b = \frac{gh_s}{\theta_s} \left( \frac{\theta_{vs} - \theta_{vg}}{U_s^2 + V_s^2 + V_c^2} \right), \quad (15)$$

$$u_* = k \frac{(U_s^2 + V_s^2 + V_c^2)^{1/2}}{\log\left(\frac{h_s}{z_0}\right) - \psi_m}, \quad \text{and} \quad (16)$$

$$\frac{m}{L} = k \frac{(\theta_s - \theta_g)}{\log\left(\frac{h_s}{z_0}\right) - \psi_h}. \quad (17)$$

Von Kármán constant  $k$  is 0.4 and convective velocity is accounted for as follow:

$$V_c = \begin{cases} 2(\theta_{vg} - \theta_{vs}), & \text{if } \theta_{vg} \geq \theta_{sg} \\ 0, & \text{if } \theta_{vg} < \theta_{sg} \end{cases}. \quad (18)$$

The quantity  $h/L$  is calculated using potential temperature at the lowest model level ( $\theta_{vs}$ ), friction velocity ( $u_*$ ) and friction potential temperature ( $h/L$ ).  $h/L$  is simply calculated using only  $Ri_b$  when friction velocity is smaller than 0.01, and  $z/L$  is calculated from  $h/L$ . The upper and lower limits are 0 and -10 for  $h/L$  and

$(z/h_s) \times (h/L)$ . For stability functions,  $\psi_{m,h} < 0.9 \times \log(h_s/z_0)$  and  $\psi_{mz,hz} < 0.9 \times \log(z/z_0)$ . Because  $\psi_{m,h}$  is a function of  $h/L$ , and  $h/L$  is a function of  $h/L$  which depends on  $\psi_{m,h}$ , solving above equations requires use of iterations after putting  $\psi_{m,h} = 0$  at first. The current code was modified not to use look-up table which is necessary for the iteration method, but to use continuous functions without any iterations. Practically, in the code flow, the roughness length is first computed based on season and land use, and then potential temperatures, velocities, bulk Richardson number, atmospheric stability regime, stability functions, the values of wind and mass variables at 2 or 10 m height.

The tangent-linear operator of a forward model analytically computes output perturbations corresponding to the input perturbations with a computational cost typically only about twice as much as that of the forward model. The adjoint of the tangent-linear operators analytically computes the sensitivity with respect to the inputs from the sensitivity with respect to the outputs (Errico 1997).

For practical implementation, some modification was made to the original forward model developed at NCAR-MM5/3DVAR (Barker et al. 2004). For the moment, the adjoint of this forward model was not used, because of modifications made to the tangent linear model so that it would work in GSI. Because only a small number of input perturbations are required (lowest level wind, temperature and moisture, and skin temperature), it is easier, and computationally less expensive to compute a sensitivity vector from the tangent linear model alone, by calling it once for each perturbation input variable set to unity, with the remaining set to zero (applying the tangent linear model to the identity matrix). Since we currently use this model only for 2 meter temperature, there results one sensitivity vector for each observation. The adjoint is merely the transpose of this vector applied to a 2-meter temperature variable to return to input values of wind, temperature and moisture.

It was also found that the forward tangent linear model was much too sensitive to the input wind perturbations, so the sensitivity to wind is currently set to zero. This extreme sensitivity results in very unrealistic analyses. One possible cause of this is that the forward model is not smooth—there are four stability regimes, with abrupt switches

between regimes, depending on vertical gradients of wind, temperature and moisture. This is well known to cause problems with tangent linear and adjoint models because branches in a program lead to discontinuities in derivatives.

The above discussion applies only to the tangent linear model and adjoint. The unmodified full nonlinear forward model is used at the beginning of each outer loop to compute pseudo-observations which are compared to the real observations.

### *b. Application results and discussion*

Figure 14 compares horizontal distribution of observation sites with large observation increments when the old and the new forward operators were used for the eastern domain at 1800 UTC 23 June 2005. With the comprehensive forward operator, the number of sites which have large innovations decreased. The large innovations in the large cities were reduced.

Figure 15 shows innovations of the surface temperature data as a function of surface pressure difference (DP) between model and sites when the old and the new forward operator were used. The general features are quite similar for the two operators, but the bias was reduced. This improvement occurred in all surface data types. It is noted that the bias even reduced over negative DP categories that mean the observation sites are located below the model surface. The score is worse over sea because the setting of  $z=2$  m is not the height of buoy (or ship) over water, and roughness is variable because of ocean wave effect. In this case, the total bias was greatly reduced from 2.2 to 0.9. According to results, such innovation improvement is prominent in the western and eastern domain which have more mountainous area compared with the central domain (not shown).

The new forward operator with the similarity theory has been tested in the NCEP GSI system since July 2005. In table 2, we compare the statistical analyses derived from the parallel run against the existing GSI system. The scores for temperature increments, calculated for the surface temperature data over the corresponding model domains, show encouraging results for use of the new forward model.

Figure 16 shows results for single-time analysis experiments with the full

implementation of the similarity theory based observation operator in the inner minimization loop. The figure is analysis differences between AN5 using old and new forward models when all available surface data are used. It can be seen that the new forward operator and its adjoint version are working in the direction of reducing the extensive analysis increments shown in Figs. 4, 5 and 7. Note that this reduction is opposite impact compared to that by use of regional background error statistics and is much larger in magnitude than that by the nonlinear QC in Fig. 8. As a result, the bull's eye features that were previously seen in the analysis increment fields (Figs 4, 5 and 7) are eliminated. This seems encouraging and reasonable because the full implementation of the new operator decreases the excessive amplification caused by addition of land surface temperature data.

Based on the results presented above, cycling experiments were carried out during Sep 24 – Oct 11 2005. Cycling period is 12 hour from 00 to 12 UTC with 6-hour interval each day. Model domain is the central 8 km NCEP WRF-NMM. The observation type 180, 182 and 187 surface data are used. Figure 17 shows time series of first-guess fit to METAR data (type 187) during cycling. At 00 UTC, control runs and experimental runs use the same first-guess but obtain different analyses at 06 and 12 UTC. When the new forward model is used, mean bias for all cycling case is increased from -0.003 to -0.405, but the value itself is not so big. Mean RMS error is 2.558 and improved from old forward model (2.574). Especially, in the second half part, the new forward model outperforms the old forward model and shows much better performance. RMS errors at final time of each short assimilation also show the improvement brought by the new forward model: 11 cases among 18 show better results. All these results are encouraging considering difference in similarity functions between NCEP WRF-NMM model surface layer physics (Chen et al. 1997) and the introduced forward model. This can imply that tangent-linear assumption is not bad in spite of high nonlinearity and complexity of the new forward model. Since currently adjoint code is simplified in the manner of satellite data assimilation, further study is required in order to use it in the inner loop of minimization process. The effect of nonlinear QC on the cycling run was almost neutral and does not show clear improvement in the first-guess fit to observation.

#### 4. Summary and concluding remarks

The U.S. near-surface observation network provides meteorological observations with high spatial resolution and temporal frequency. In this paper, we tested assimilation of near-surface temperature data in the NCEP regional Gridpoint Statistical-Interpolation (GSI). The single-time analysis experiments showed the analysis field contains smaller and detailed structures as METAR or mesonet data are added. The comparisons of analysis field against radiosonde soundings supported the usefulness of land surface temperature data.

The use of surface observations is very sensitive to the background error covariance used in the 3D variational analysis. In the existing approach, horizontal scales of the background error are estimated from derivatives, but in the new approach, these are estimated using auto-covariances (Wu 2005). Both approaches use the NMC method, with global model forecasts for the existing approach and regional model forecasts for the new approach. For the global derived background error, the correlation length scales and background variances are a function of latitude and vertical. In the new background error, the scales of the structure function vary in the vertical but are no longer latitude dependent for statistical robustness. The use of new regional background error statistics showed the overall pattern is similar to the control run but the amplitude is more intensified in the analysis increment fields. It is believed to be the results of smaller vertical structures in the regional background error covariances. The use of nonlinear QC, turned on for the complete second outer loop, showed somewhat promising result in some cases by reducing excessive analysis increment.

Accumulated statistics of observation innovation evaluated during May 2005 for each 8 km mesoscale model domain was useful to understand the characteristics of the observed - guess statistics for the surface temperature data. According to the statistics, surface mesonet temperature data were found to have a considerable amount of outliers compared with other land surface temperature data such as METAR and synoptic land/sea data. Use of mesonet uselist and monitoring of observation innovation on a station-by-station and variable-by-variable basis was proposed as a short- and long-term method, respectively, to solve the problems. The nighttime western and central domains

indicated a model warm bias. The western domain, in particular, showed a model warm bias of about +2.2 °C at nighttime when compared with the eastern domain which did not show any obvious bias. Stations with large innovations are distributed uniformly in the nighttime western and central domains, while they are mainly located in the large cities in the daytime eastern domain.

Sources of disagreement between observations and model include observation errors and errors related to the model. It is shown that the latter can be reduced by introducing a more comprehensive forward model in the NCEP GSI analysis system. The implementation of the new forward model involved two aspects: the non-linear model to compute the innovations and the use of the adjoint to compute the sensitivity vector. In the inter-comparison of the old and new forward operators using case experiments and long term runs, the comprehensive forward model is shown to improve the innovation statistics. This seems to be due to the realistic considerations of surface characteristics (e.g., roughness length) and atmospheric stability within surface layer. The parallel run results during July to August 2005 also showed the new comprehensive forward model reduced bias in the innovations, especially, over the mountainous western U. S. domain. The effect was more remarkable for stations below model surface. In the short assimilation experiments of 6-hour interval, mean RMS error was improved from 2.574 to 2.558 by introduction of the new forward model; Use of nonlinear QC with the old forward model had neutral impact. In the short assimilation experiment, the improvement brought by the new forward model in the short-range and near-surface temperatures is rather small compared to the old one. The possible main reason is thought to be the short forecast range (6 hour). The performance of the new forward model was found to have dependency on the horizontal resolution of first-guess field and would produce worse analyses in case of coarser (e.g., 12 km) background resolution (now shown here). Thus, a study of the impact on longer forecast ranges (12 hour and 24 hour for instance) and different background resolutions could be carried out in the future.

The new operator has a potential to assimilation of diverse surface data in the NCEP regional GSI system. It can be applied to surface GSI 2D-VAR which is a surface analysis method under development in the NCEP now. Because GSI 2D-VAR does not require tangent-linear and adjoint models, it can gain much profit from the encouraging

effect of the new forward model on the innovation statistics (Pondeca 2005, personal communication). It can be used for not only near-surface data over and but also satellite data, such as QuikSCAT sea surface wind. Although we showed it is undesirable to apply the new forward model to sea data because the height of buoy (or ship) data is not fixed due to ocean wave effect, roughness length from ocean model is worth considerable.

Ultimately, consistency between near-surface forward model and model surface layer scheme should be considered although there is not much difference between diverse surface layer similarity functions. Since there are no available tangent-linear and adjoint models corresponding to the current NCEP WRF-NMM surface layer physics, development of them is thought to be an encouraging task. Because the near-surface data assimilation used in this paper is based on Dyer and Hicks formula which has been used in the MRF PBL scheme, the assimilation and prediction system are expected to produce better performance if the MRF PBL scheme are used as a boundary layer parameterization scheme. Other future tasks include improvement of adjoint code, connection of the new forward model with nonlinear QC to the land surface data, and linkage with anisotropic background error covariances.

## Acknowledgments

The first author would like to thank KMA for funding this work through its visiting scientist program. The first author would also like to thank the many people from KMA/NWPD and NCEP/EMC that have made this project possible. The support and encouragement of Drs. Woo-Jin Lee and Stephen J. Lord are appreciated. Useful comments on this paper were provided by Drs. Geoff DiMego, John Derber, Manuel Pondeva, Russ Treadon and Kenneth Mitchell. Dr. Stephane Laroche at Canadian Meteorological Center also provided us valuable comments. The kind assistance of Dennis Keyser, Stacie Bender and Daryl Kleist are appreciated.

## References

- Andersson, E. and H. Järvinen, 1999: Variational quality control. *Quart. J. Roy. Meteor. Soc.*, **125**, 697-722.
- Barker, D. M., W. Huang, Y.-R. Guo, A. J. Bourgeois, and Q. N. Xiao, 2004: A three-dimensional variational data assimilation system for MM5: implementation and initial results. *Mon. Wea. Rev.*, **132**, 897-914.
- Benjamin, S. G., and Coauthors, 2004: An hourly assimilation-forecast cycle: The RUC. *Mon. Wea. Rev.*, **132**, 495-518.
- Burgman, K., 1979: Multivariate analysis of temperature and winds using optimum interpolation. *Mon. Wea. Rev.*, **107**, 1423-1444.
- Chen, F., Z. Janjic', and K. Mitchell, 1997: Impact of atmospheric surface-layer parameterizations in the new land-surface scheme of the NCEP mesoscale Eta model. *Boun.-Layer Meteorol.* **85**, 391-421.
- COMET Program updated, 2005: Understanding Data Assimilation: How Models Create Their Initial Conditions [Available online at <http://meted.ucar.edu/nwp/pcu1/ic6/frameset.htm>].

- Derber, J. C., D. F. Parrish, and S. J. Lord, 1991: The new global operational analysis system at the National Meteorological Center. *Wea. Forecasting*, **6**, 538-547.
- Dey, C. H., and L. L. Morone, 1985: Evolution of the National Meteorological Center global data assimilation system: January 1982-December 1983. *Mon. Wea. Rev.*, **113**, 304-318.
- DiMego, G. J., 1988: The National Meteorological Center Regional Analysis System. *Mon. Wea. Rev.*, **116**, 977-1000.
- \_\_\_\_\_, G. J., Y. Lin, M. Pondeva, S.-J. Lee, 2005: The real-time mesoscale analysis (RTMA) - A first step towards an analysis of record. *Science and Technology Seminar*, 5 October 2005, Washington, DC, USA. [Available online at [http://www.nws.noaa.gov/mdl/seminar/s&t\\_seminar2.htm](http://www.nws.noaa.gov/mdl/seminar/s&t_seminar2.htm).]
- Doswell, C. A., and S. Lasher-Trapp, 1997: On measuring the degree of irregularity in an observing network. *J. Atmos. Oceanic Technol.*, **14**, 120-132
- Dyer, A. J., and B. B. Hicks, 1970: Flux-gradient relationships in the constant flux layer. *Quart. J. Roy. Meteor. Soc.*, **96**: 715-721.
- Errico, R. M., 1997: What is an adjoint? *Bull. Amer. Meteor. Soc.*, **78**, 2577-2591.
- Guo, Y.-R., D.-H. Shin, J.-H. Lee, Q.-N. Xiao, D. M. Barker, and Y.-H. Kuo, 2002: Application of the MM5 3DVAR system for a heavy rain case over the Korean Peninsula. *PSU/NCAR Mesoscale Model Users' Workshop*, Boulder, CO, NCAR. [Available online at <http://www.mmm.ucar.edu/mm5/workshop/ws02/Guo.pdf>.]
- Hong, S.-Y., and H.-L. Pan, 1996: Nonlocal boundary layer vertical diffusion in a medium-range forecast model. *Mon. Wea. Rev.*, **124**, 2322-2339.
- Janjic, Z. I., J. P. Gerrity, and S. Nickovic, 2001: An alternative approach to nonhydrostatic modeling. *Mon. Wea. Rev.*, **129**, 1164-1178.
- Kanamitsu, M., 1989: Description of the NMC global data assimilation and forecast system. *Wea. Forecasting*, **4**, 335-342.
- Kimeldorf, G., and G. Wahba, 1970: A correspondence between Bayesian estimation of stochastic processes and smoothing by splines. *Ann. Math. Stat.*, **41**, 495-502.
- Lee, S.-J., D. F. Parrish, W.-S. Wu, M. Pondeva, D. Keyser, and G. DiMego, 2005: Use of surface mesonet data in the NCEP regional gridpoint statistical-interpolation (GSI) system. *21st Conference on Weather Analysis and Forecasting/17th*

- Conference on Numerical Weather Prediction*, 1-5 August 2005, Washington, DC.  
[Available online at [http://ams.confex.com/ams/WAFNWP34BC/techprogram/paper\\_95238.htm](http://ams.confex.com/ams/WAFNWP34BC/techprogram/paper_95238.htm).]
- Lorenc, A. C., 1986: Analysis methods for numerical weather prediction. *Quart. J. Roy. Meteor. Soc.*, **112**, 1177-1194.
- Myrick, D. T., J. D. Horel, and S. M. Lazarus, 2005: Local adjustment of the background error correlation for surface analyses over complex terrain. *Wea. Forecasting*, **20**, 149-160.
- Parrish, D. F., and J. C. Derber, 1992: The National Meteorological Center's Spectral Statistical-Interpolation analysis system. *Mon. Wea. Rev.*, **120**, 1747-1763.
- Purser, R. J., W.-S. Wu, D. F. Parrish, and N. M. Roberts, 2003: Numerical aspects of the application of recursive filters to variational statistical analysis. Part II: Spatially inhomogeneous and anisotropic general covariances. *Mon. Wea. Rev.*, **131**, 1536-1548.
- Ruggiero, F. H., K. D. Sashegyi, R. V. Madala, and S. Raman, 1996: The use of surface observations in four-dimensional data assimilation using a mesoscale model. *Mon. Wea. Rev.*, **124**, 1018-1033.
- \_\_\_\_\_, G. D. Modica, and A. E. Lipton, 2000: Assimilation of satellite imager data and surface observations to improve analysis of circulations forced by cloud shading contrasts. *Mon. Wea. Rev.*, **128**, 434-448.
- Urban, B., 1996: Coherent observation operators for surface data assimilation with application to snow depth. *J. Appl. Meteor.*, **35**, 258-270.
- Wade, C. G., 1987: A quality control program for surface mesometeorological data. *J. Atmos. Oceanic Technol.*, **4**, 435-453.
- Wu, W.-S., 2005: Background error for NCEP's GSI analysis in regional mode. *4th WMO International Symposium on Assimilation of Observations in Meteorology and Oceanography*, 18-22 April 2005, Prague, Czech Republic
- \_\_\_\_\_, R. J. Purser, and D. F. Parrish, 2002: Three-dimensional variational analysis with spatially inhomogeneous covariances. *Mon. Wea. Rev.*, **130**, 2905-2916.

Table 1. Summary of experimental design using synoptic sea (180), synoptic land (181), METAR (187) and mesonet (188) temperature data.

Experiment name (Analysis)	Date	Used surface T data	Background error statistics	Description
CNTL (AN1)	06 UTC 04 Feb 2005	180, 182	Global	Control run (Default option in GSI)
SYNP (AN2)	12 UTC 10 Mar 2005	180, 182, 181	Global	Impact of synoptic land data
META (AN3)	18 UTC 23 Mar 2005	180,182, 181, 187	Global	Impact of METAR data
MESO (AN4, AN4REG*)	18 UTC 23 Mar 2005	180, 182 181, 188	Global	Impact of mesonet data (* Run with regional background error statistics)
ALLD (AN5, AN5NEW**, AN4NQC***)	18 UTC 23 Mar 2005	180, 182, 181, 187, 188	Global	Impact of all surface data (** Run with the new forward model; *** Run with nonlinear quality control)

Table 2. Mean error statistics during early July 2005.

Near-surface data	Forward model	BIAS			RMSE		
		West	Central	East	West	Central	East
188	Old	-2.79	-1.03	1.73	4.57	3.70	3.73
	New	-2.17	-0.76	0.59	4.37	3.48	3.17
187	Old	-3.15	-0.53	1.59	4.68	3.32	3.26
	New	-2.15	-0.19	0.52	3.95	2.99	2.54
181	Old	-2.79	-0.90	1.23	4.17	3.52	3.22
	New	-1.81	-0.44	0.51	3.49	3.08	2.67
180	Old	-0.85	-0.49	-1.69	4.00	1.72	4.37
	New	-1.84	-1.19	-2.28	4.06	2.56	4.61

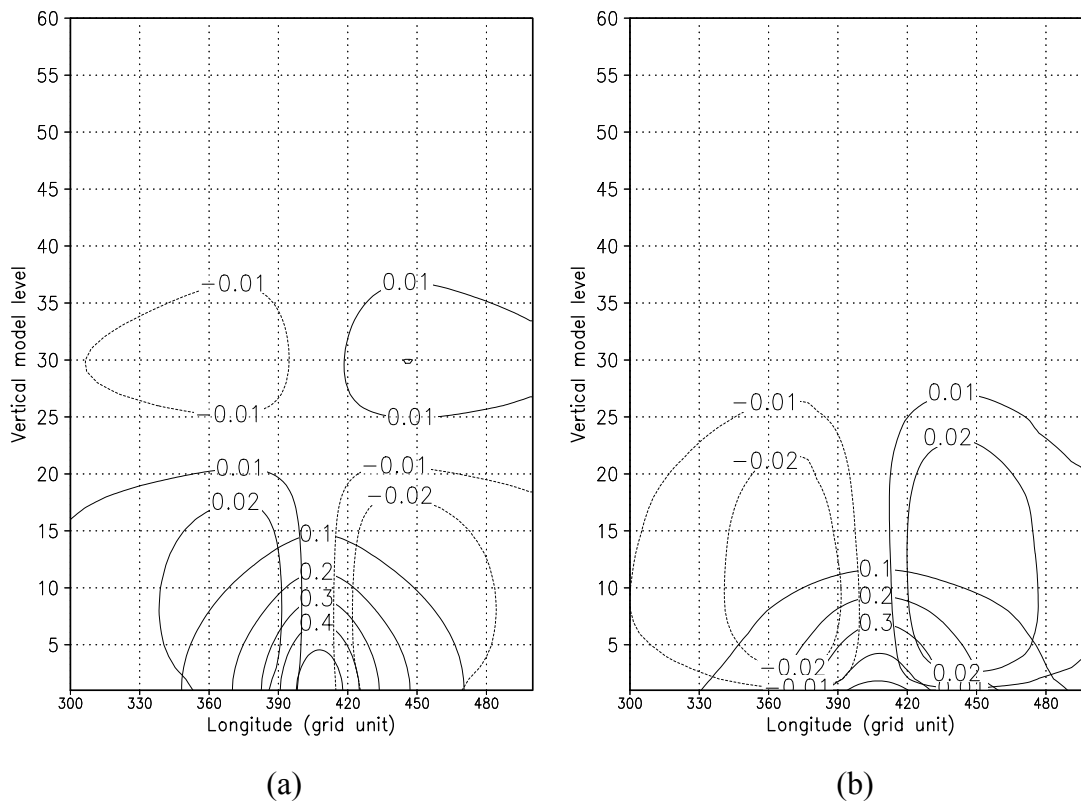


Figure 1. (a) Analysis increment for single observation at 45 N and 1000 hPa with global background statistics interpolated to regional domain. (b) same as (a) but with regional background statistics.

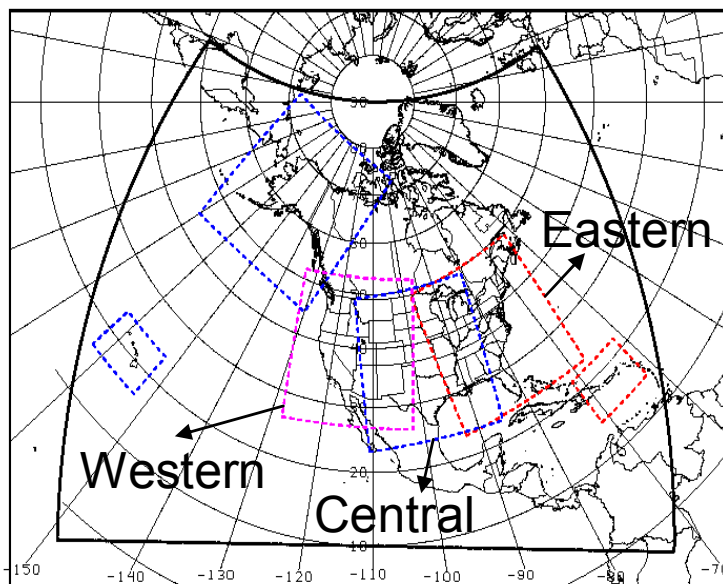
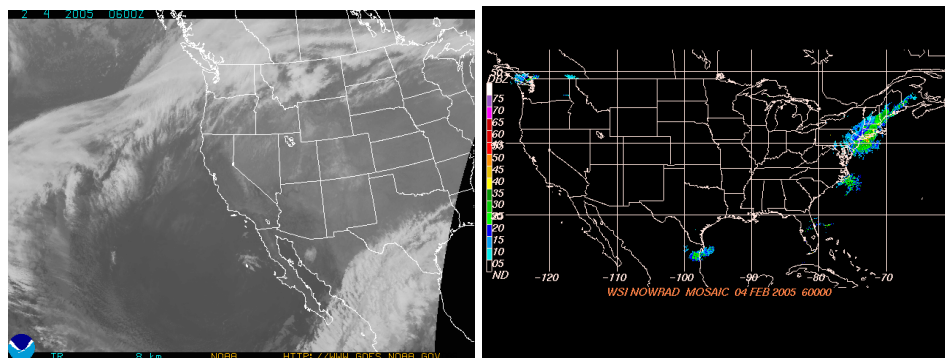
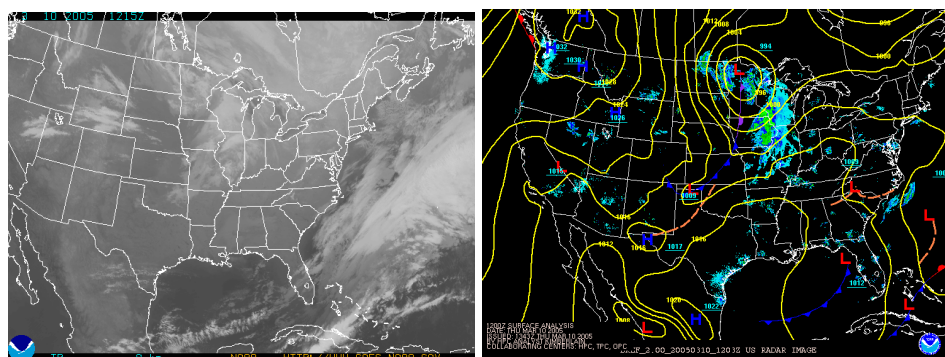


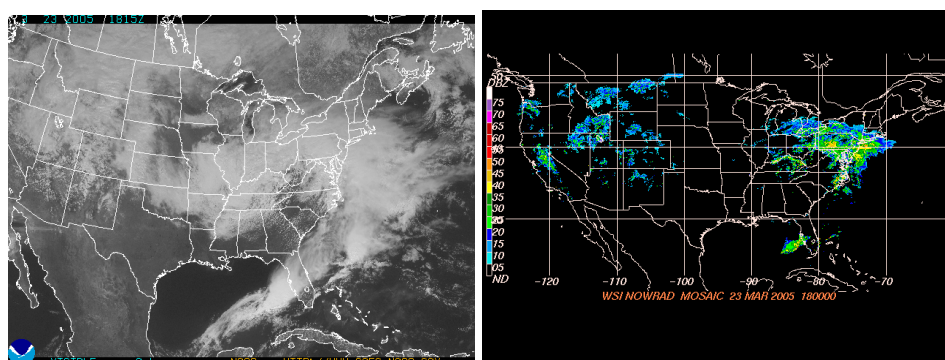
Figure 2. Nested Meso-08 domains.



(a)



(b)



(c)

Figure 3. Satellite and radar images (a) 0600 UTC 04 Feb, (b) 1200 UTC 10 Mar, and (c) 18 UTC 23 Mar 2005.

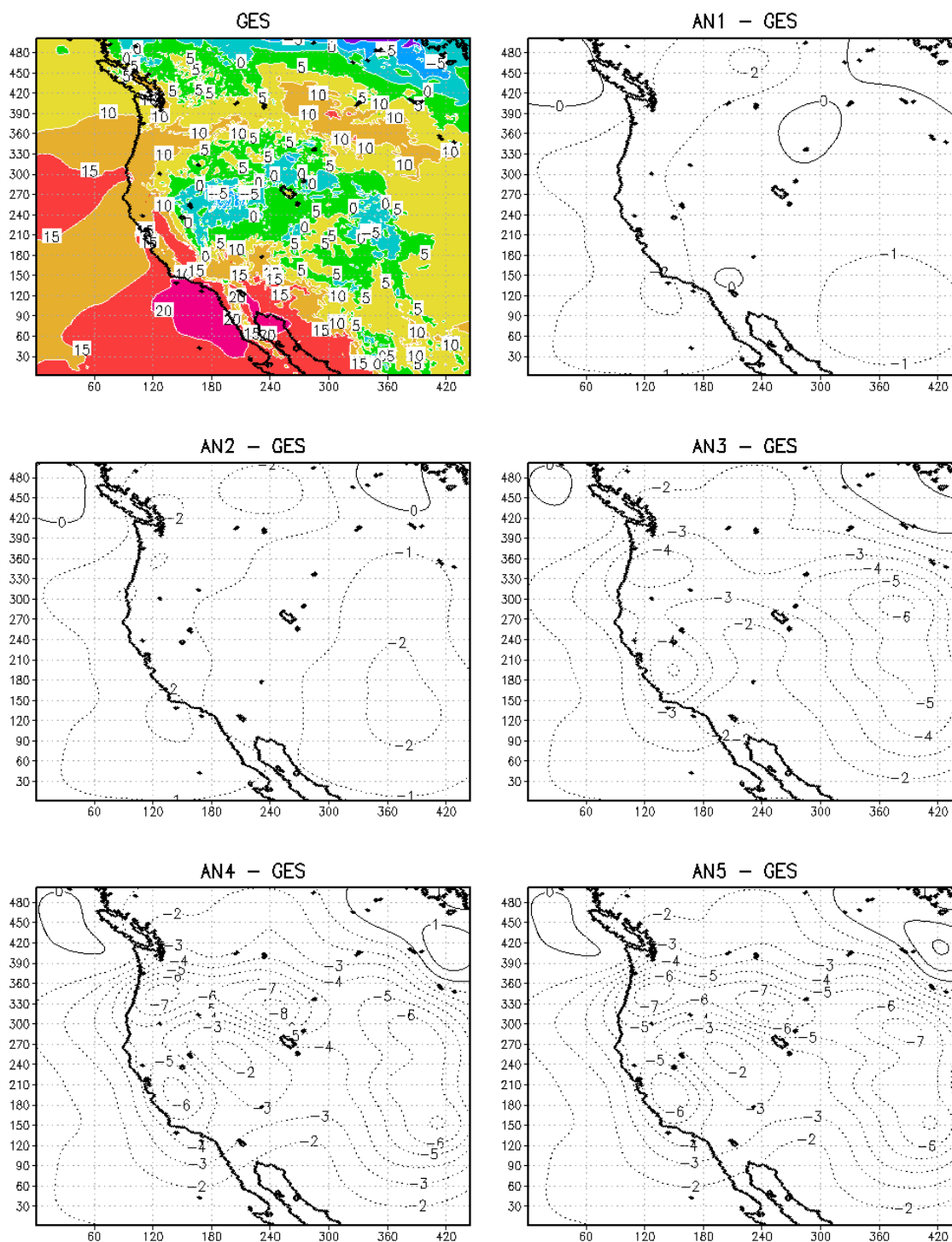


Figure 4. Horizontal fields of analysis increments for surface temperature at 0600 UTC 04 Feb 2005 (Fig. 2a).

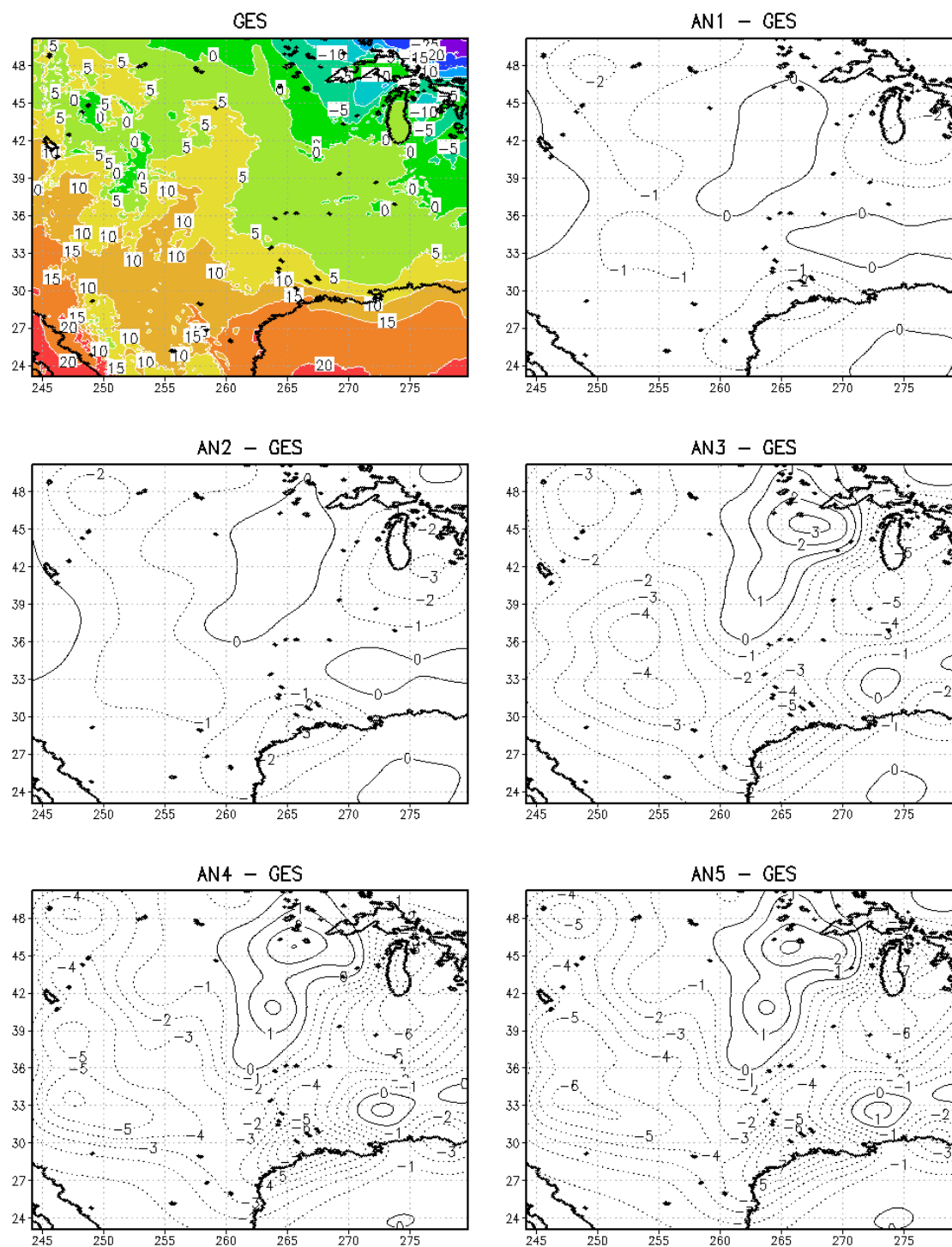


Figure 5. Same as in Fig. 4 except for 1200 UTC 10 Mar 2005 (Fig. 2b).

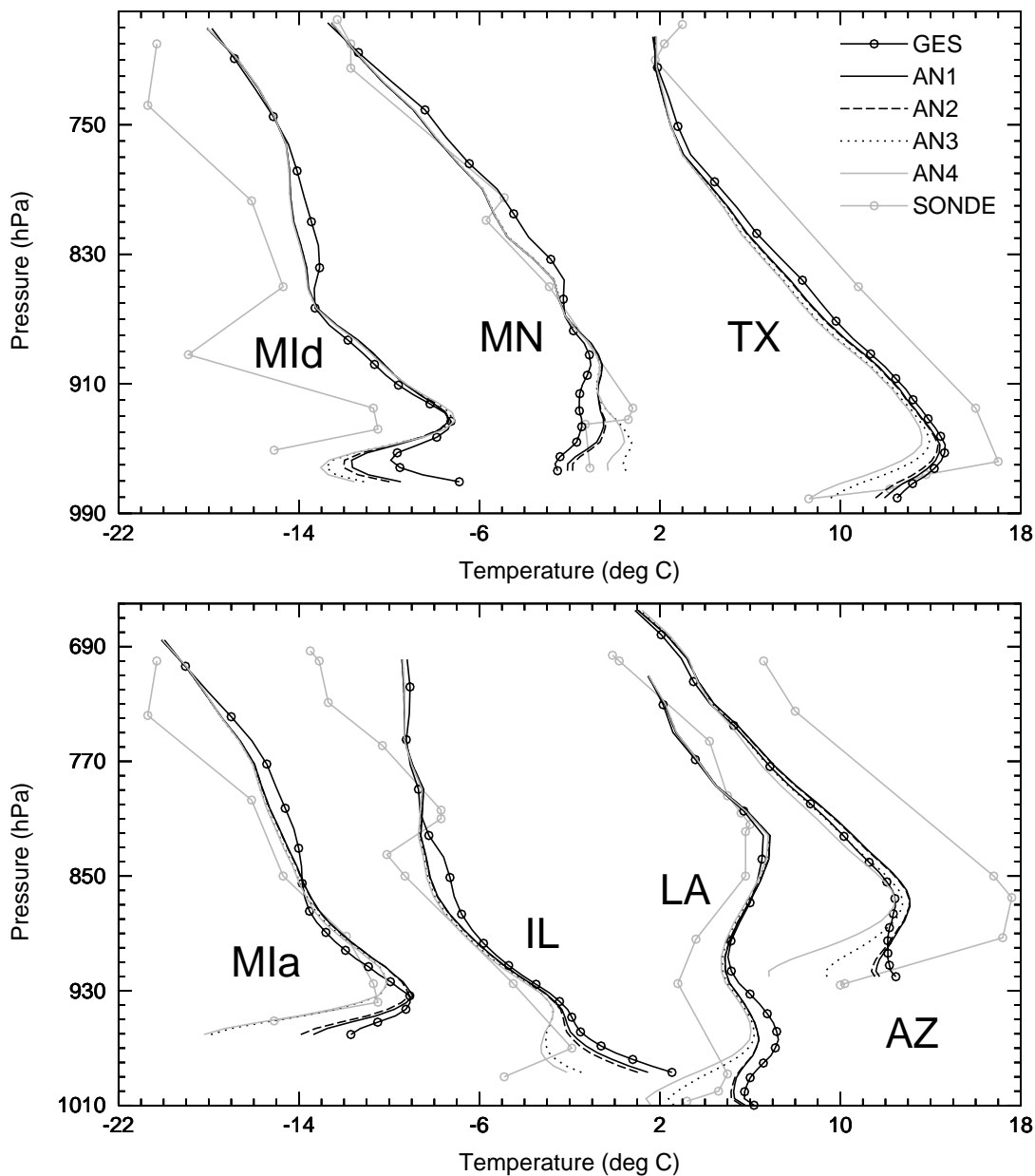


Figure 6. Comparison of analysis temperature profiles against radiosonde soundings (full gray lines with open circles) after interpolation into radiosonde sites (AZ, 32.12N 110.93W; MN, 44.83N 93.55W; Mia, 44.55N 84.43W; Mid, 42.70N 83.47W; IL, 40.15N 89.33W; LA, 32.45N 93.83W; TX, 29.37N 100.92W).

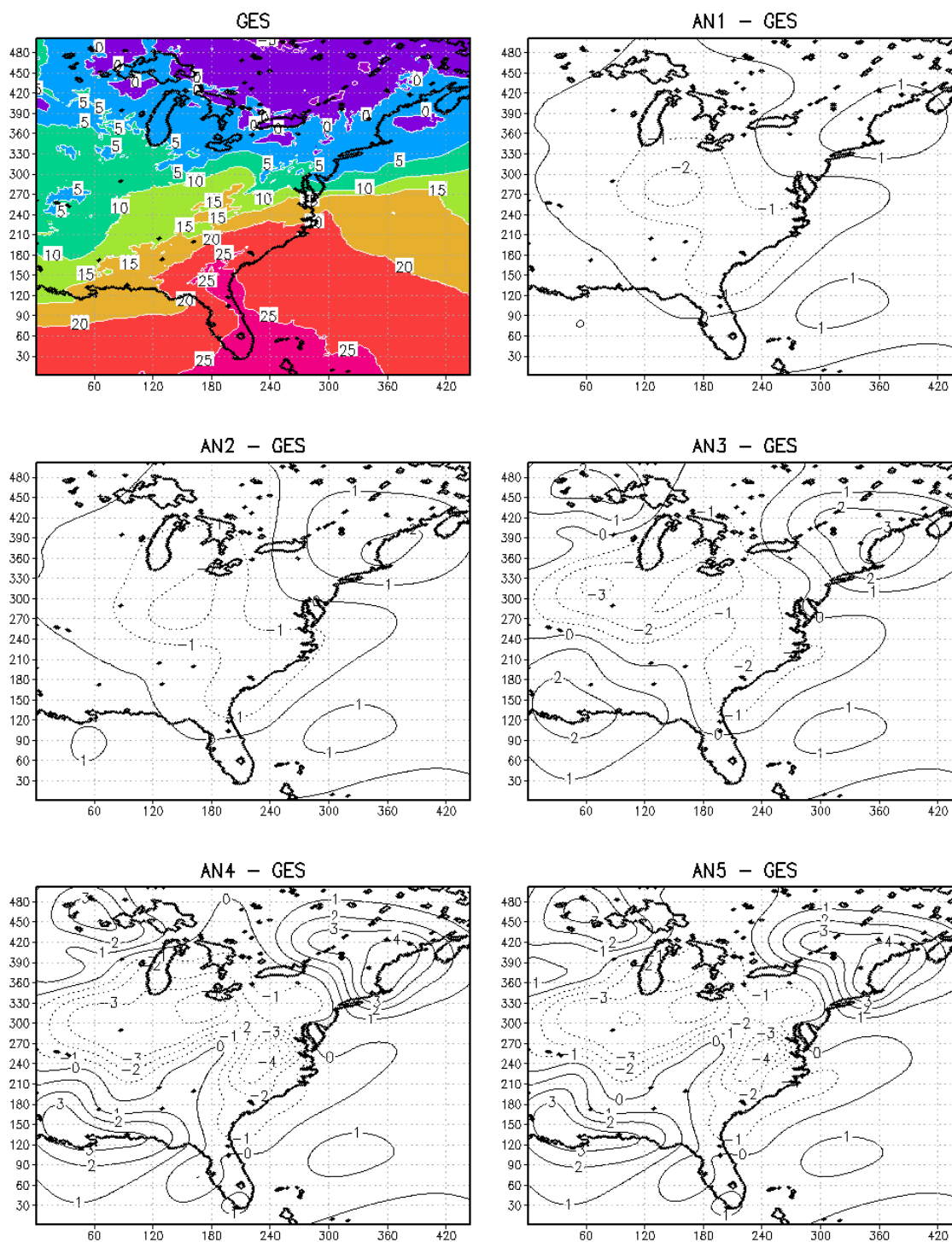


Figure 7. Same as in Fig. 3 except for 1800 UTC 23 Mar 2005 (Fig. 2c).

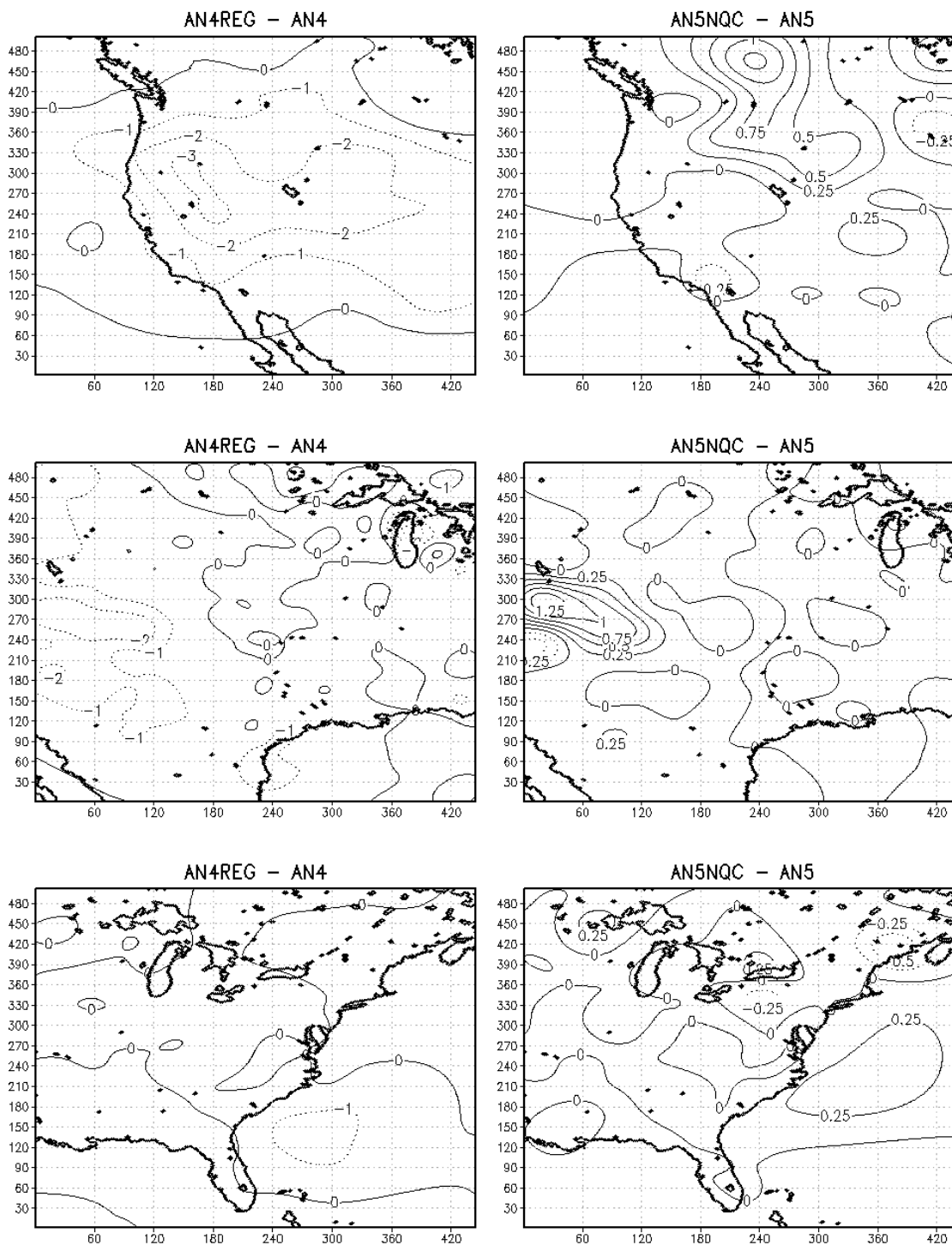


Figure 8. Analysis differences between AN4 using global and regional background error statistics (left panels). Analysis differences between AN5 using and not using non-linear quality control procedure (right panels).

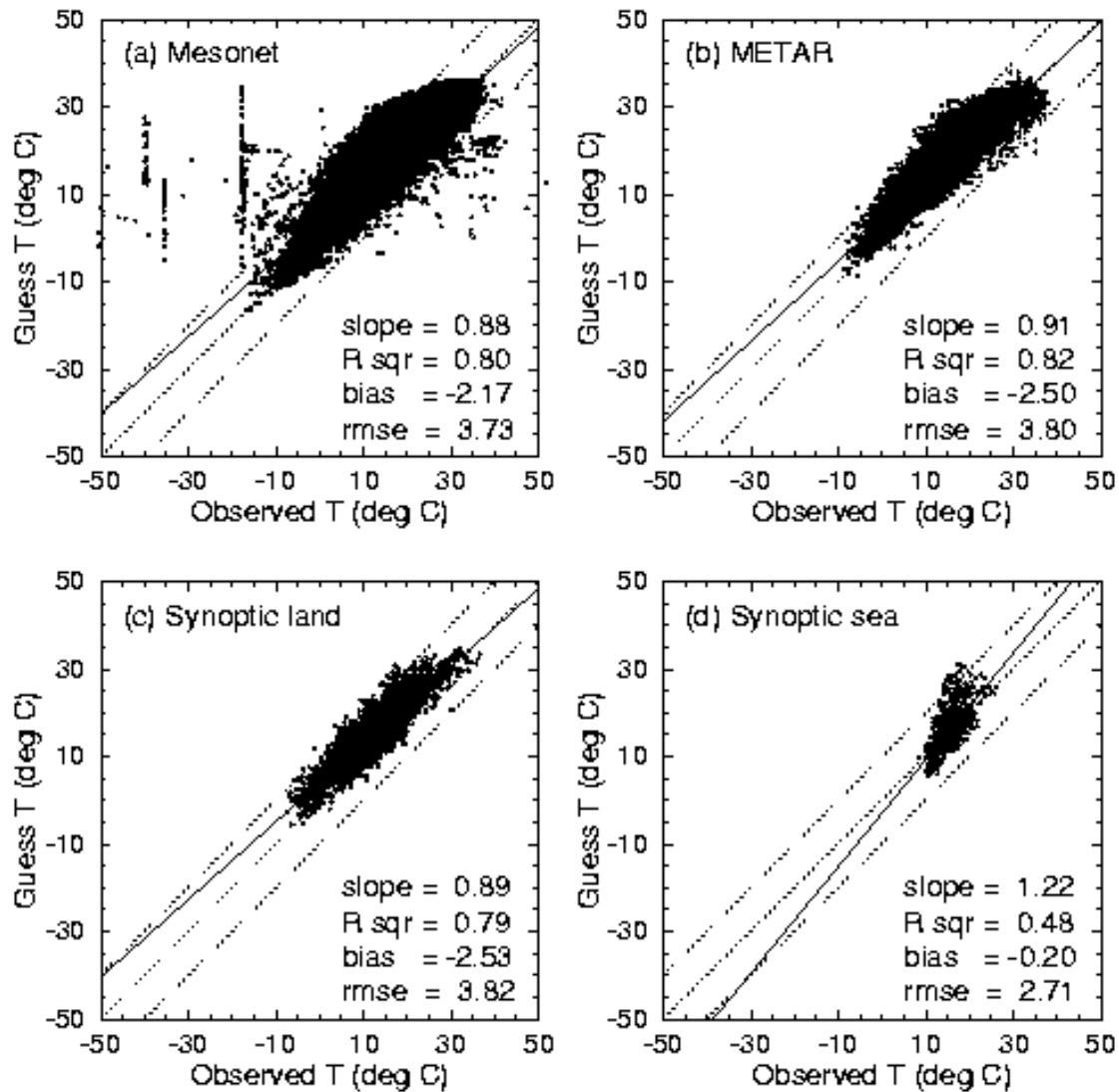


Figure 9. Scatter diagram of observed versus first-guess surface temperature ( $^{\circ}\text{C}$ ) during May 2005 for the nighttime (0600 UTC) western model domain.

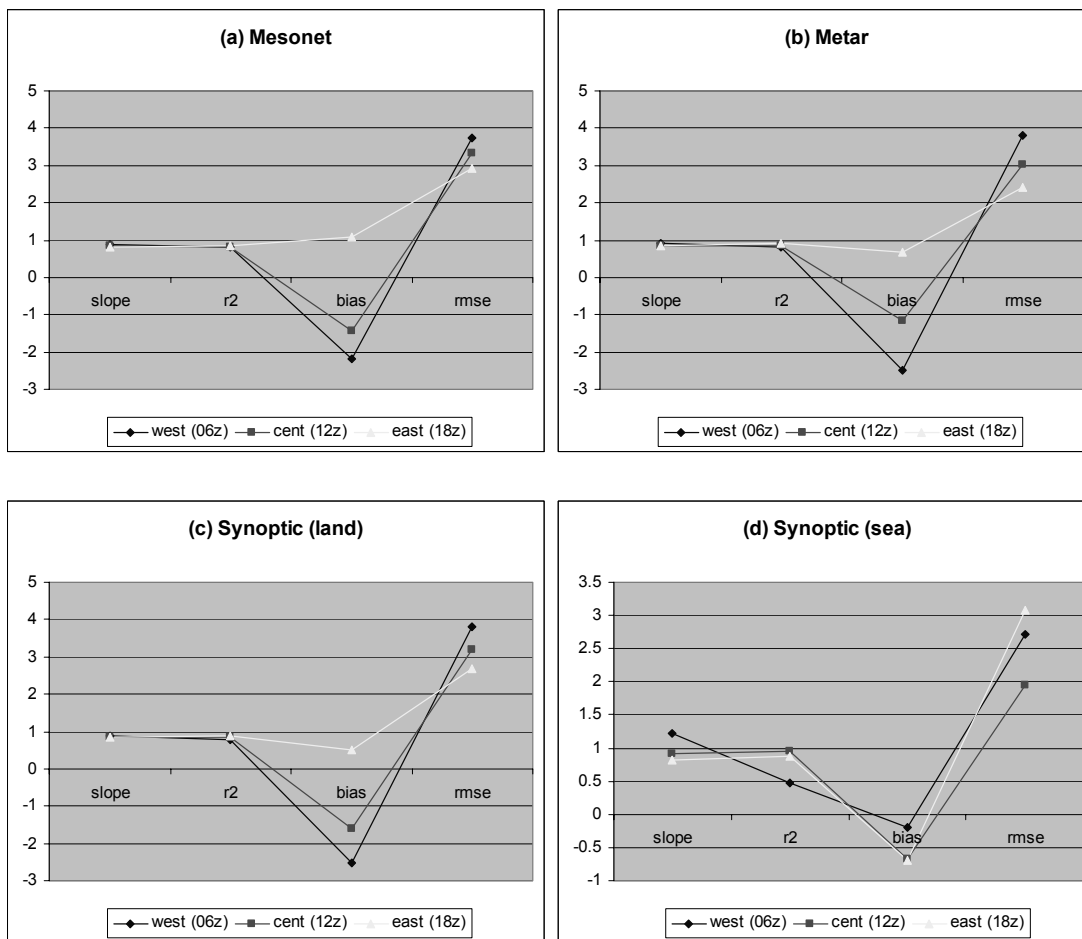


Figure 10. Comparison of (observed – guess) statistics between the three domains for surface temperature data during May 2005.

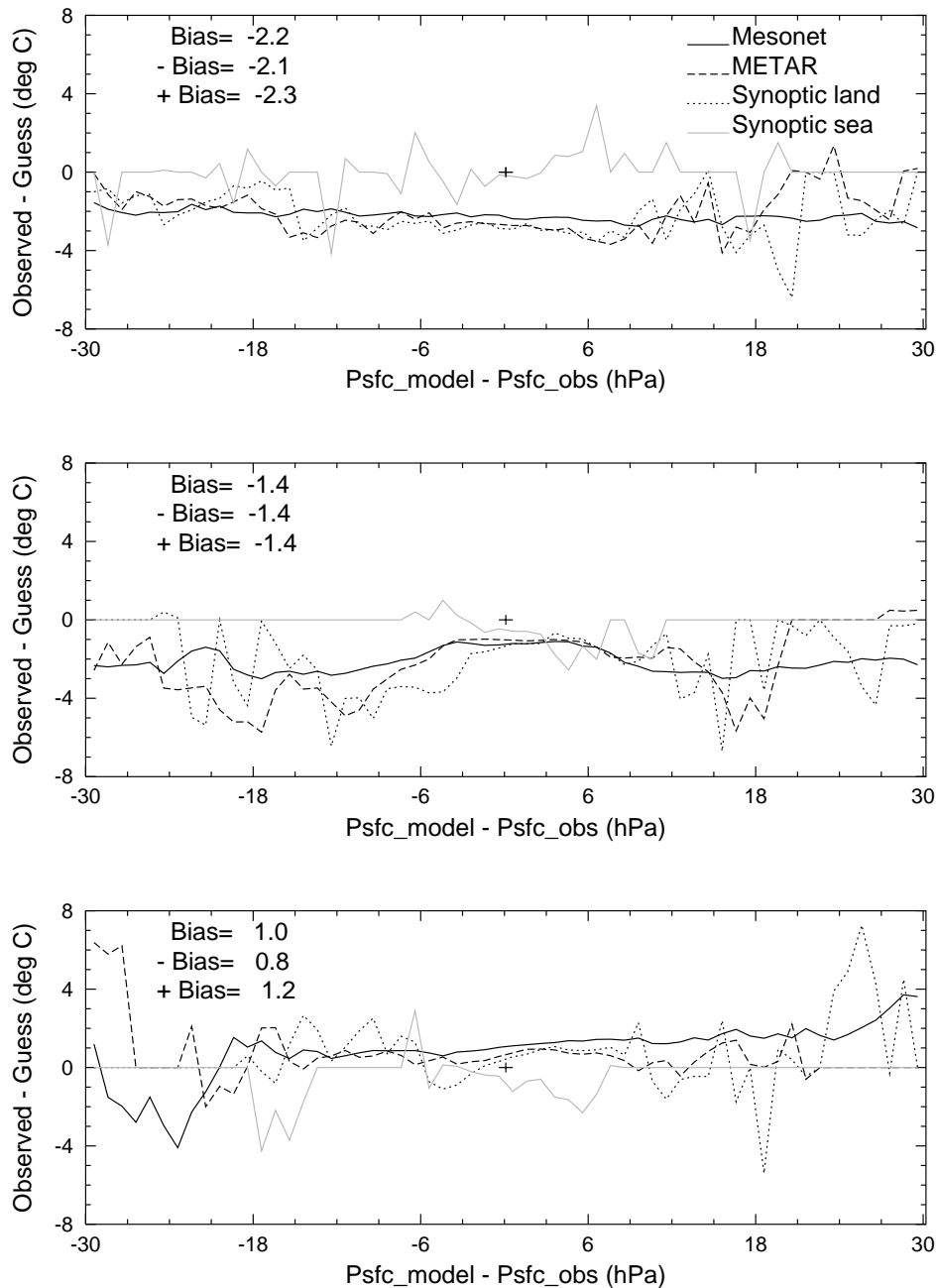


Figure 11. Mean Innovations of the surface temperature data as a function of surface pressure difference between model and observation during May 2005 for the night-time (0600 UTC) western (top), dawn-time (1200 UTC) central (middle), and day-time (1800 UTC) eastern domains (bottom).

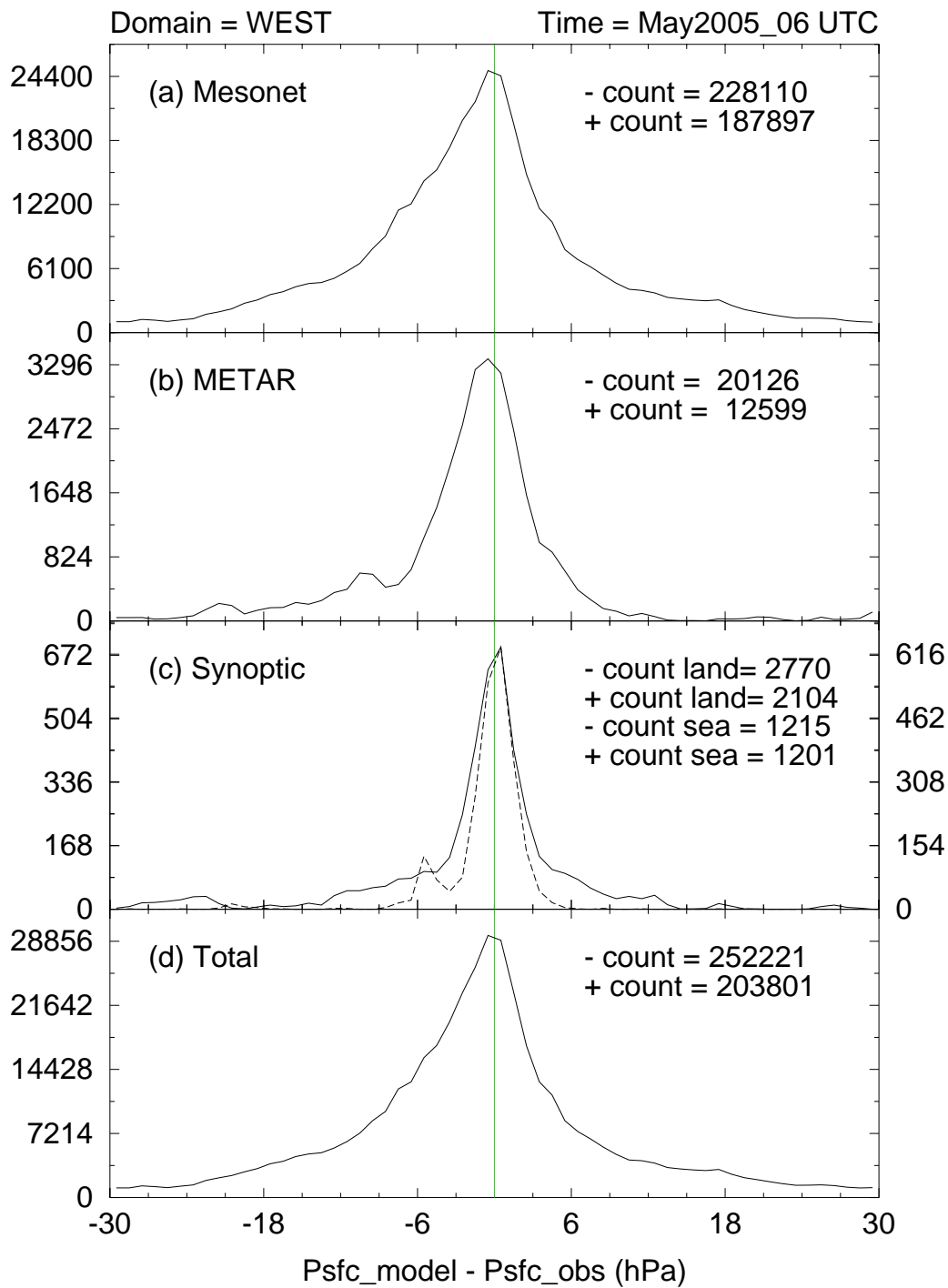


Figure 12. The number of stations as function of surface pressure difference between model and observation in the western domains at 06 UTC May 2005. The dashed line is corresponding to synoptic sea surface data which use right y-axis values.

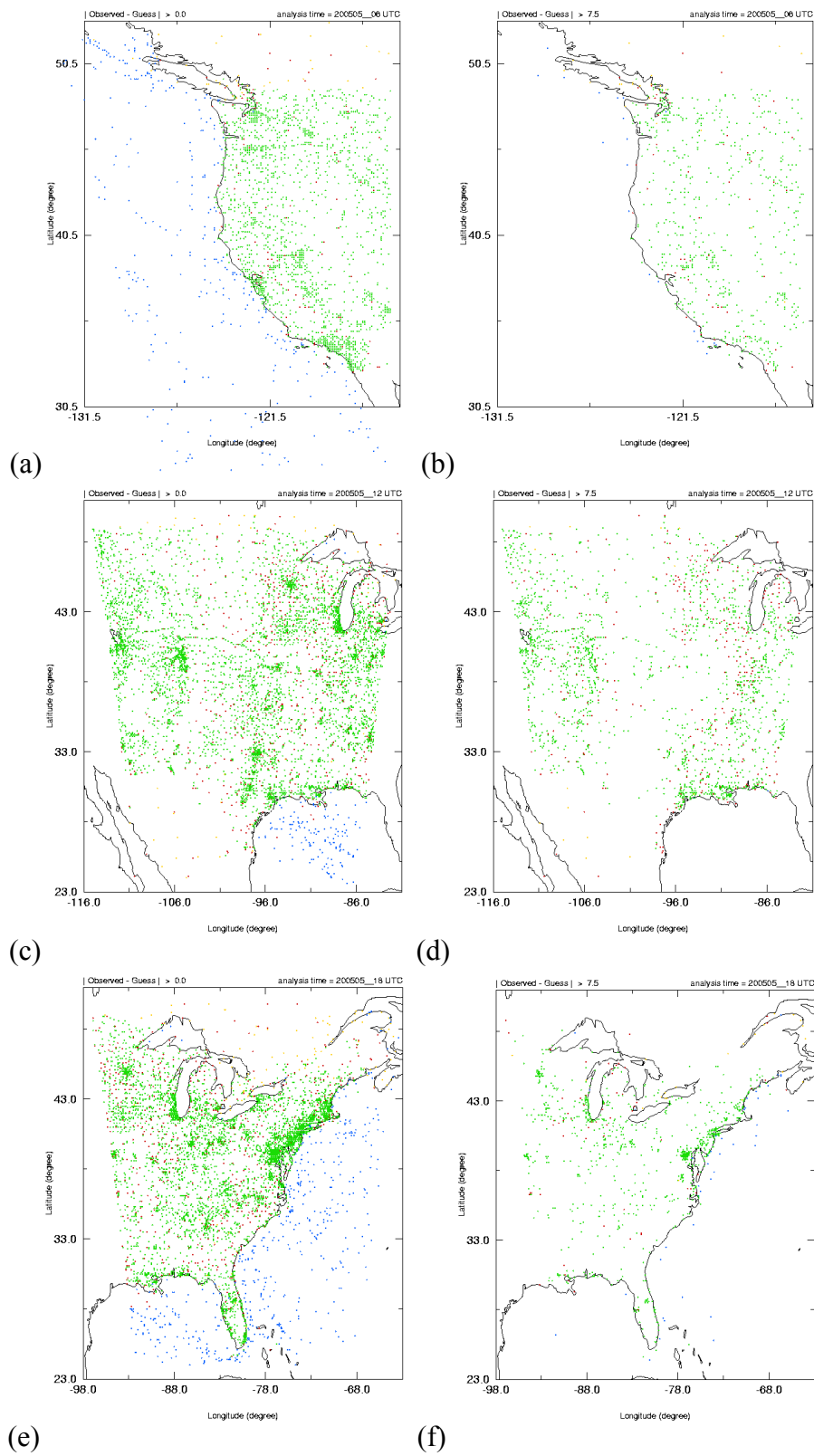


Figure 13. All surface stations (left) and large-innovation sites (right) in each domain during May 2005.

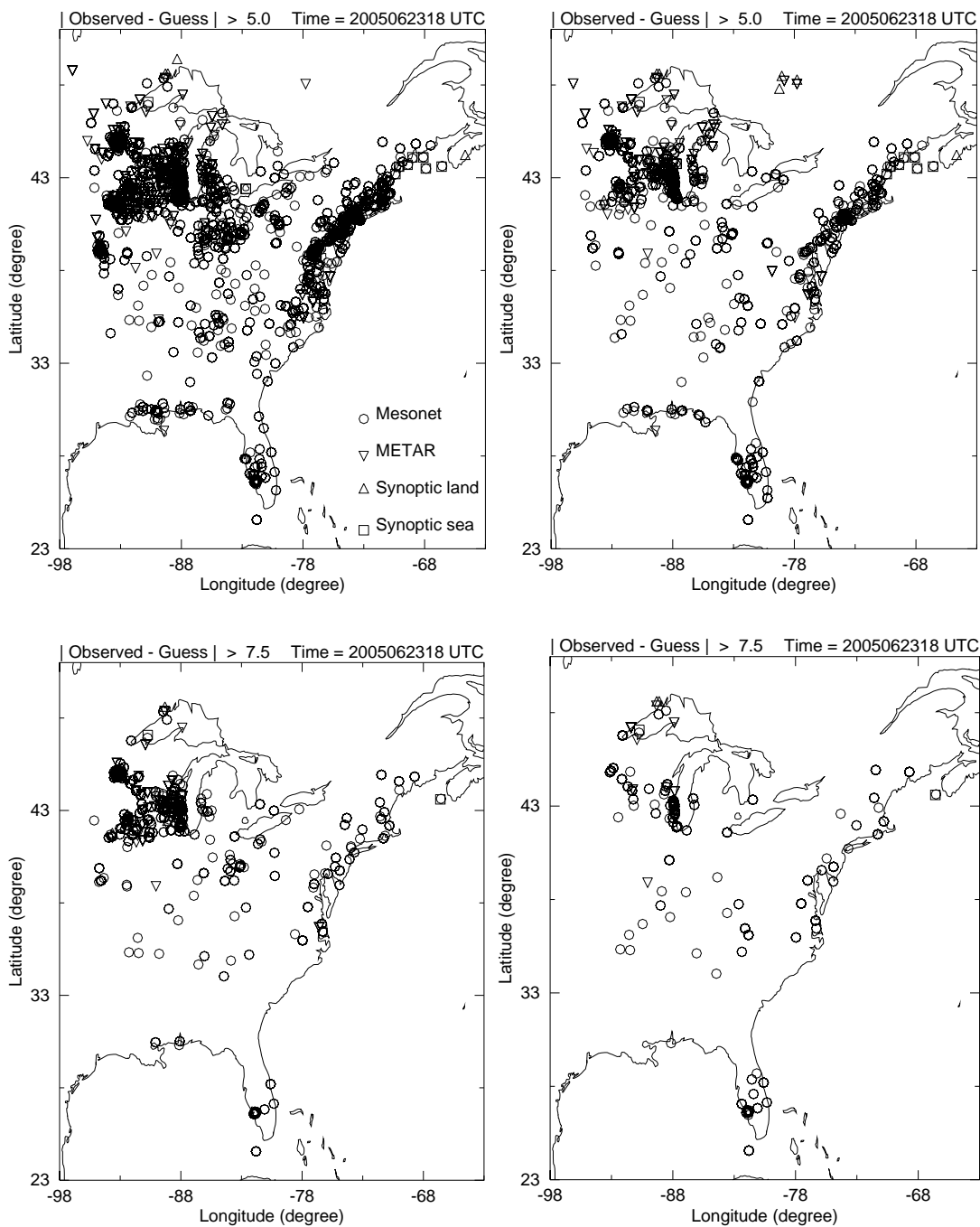


Figure 14. Distribution of large innovation sites in the eastern domain at 18 UTC 23 June 2005 using old (left panels) and new (right panels) forward models.

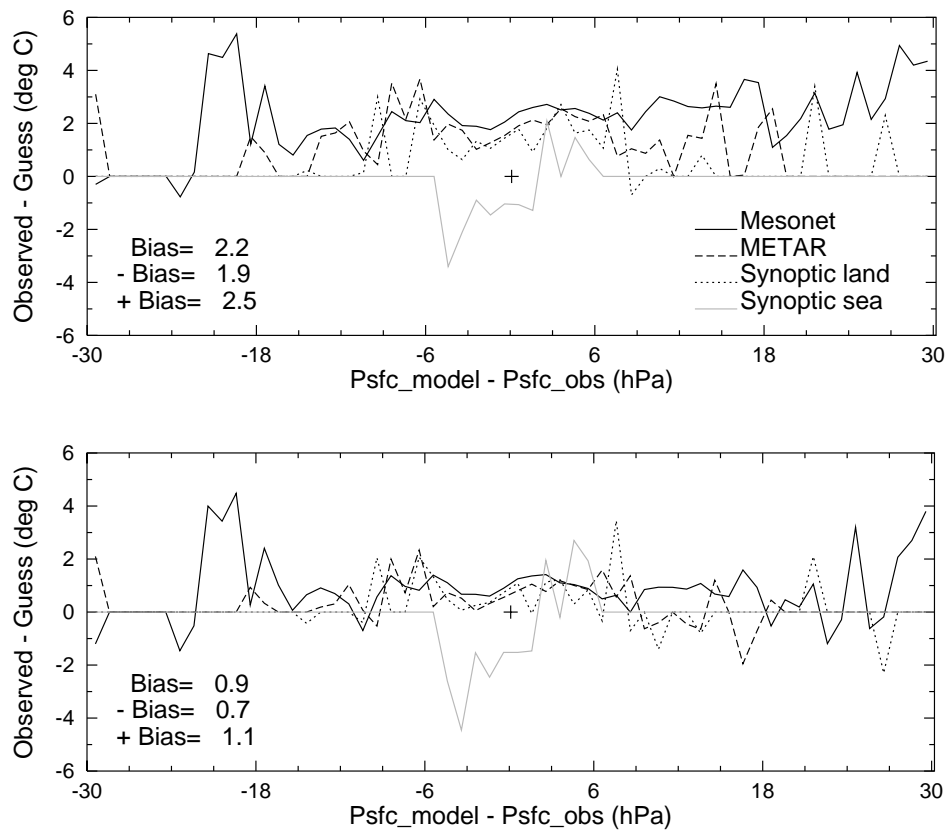


Figure 15. Observation innovation differences using old (top) and new (bottom) forward models (valid at 1800 UTC 23 June 2005). The innovations are averaged values at each surface pressure difference interval.

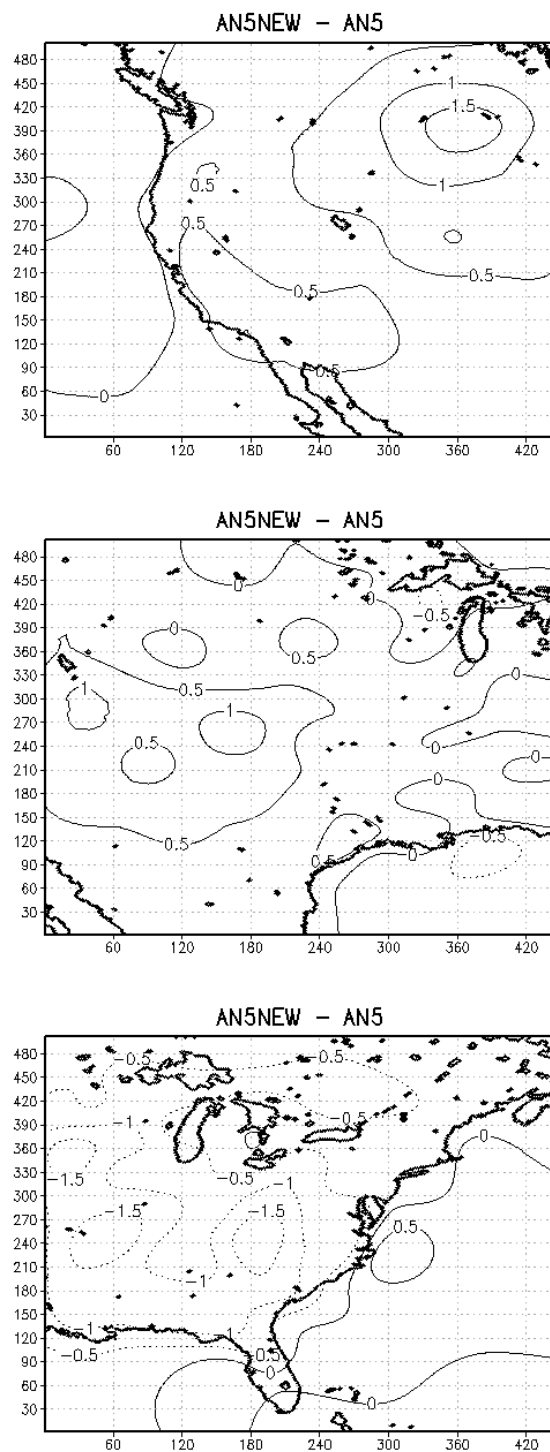


Figure 16. Analysis differences between AN5 using old and new forward models when all available surface data are used.

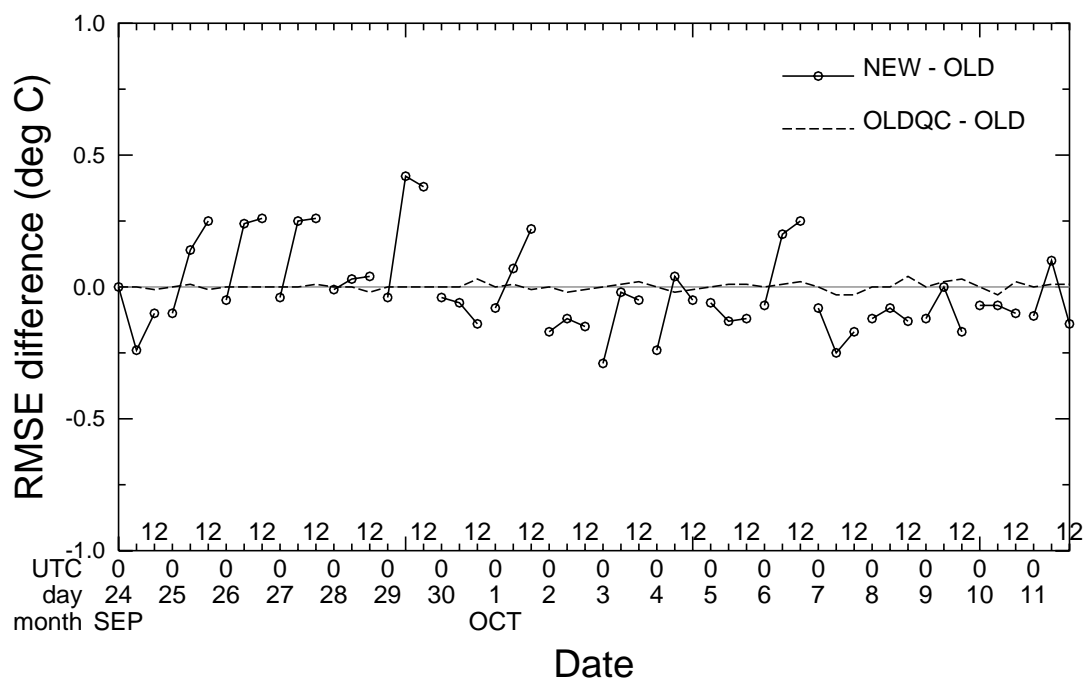


Figure 17. RMS error difference between cycling experiments. OLD and NEW mean use of old and new forward models without nonlinear QC. OLDQC means use of the old forward model with nonlinear QC.